General Disclaimer

One or more of the Following Statements may affect this Document

- This document has been reproduced from the best copy furnished by the organizational source. It is being released in the interest of making available as much information as possible.

- This document may contain data, which exceeds the sheet parameters. It was furnished in this condition by the organizational source and is the best copy available.

- This document may contain tone-on-tone or color graphs, charts and/or pictures, which have been reproduced in black and white.

- This document is paginated as submitted by the original source.

- Portions of this document are not fully legible due to the historical nature of some of the material. However, it is the best reproduction available from the original submission.

Produced by the NASA Center for Aerospace Information (CASI)

NASA CR 168067

Department of Aerospace Engineering
and Applied Mechanics
University of Cincinnati

(NASA-CR-168067) COMPRESSOR CASCADE PERFORMANCE DETERIORATION CAUSED BY SAND INGESTION (Cincinnati Univ.) 71 p
HC A04/MF A01 CSCL 01A G3/02

N83-16286
Unclas
02494

COMPRESSOR CASCADE PERFORMANCE DETERIORATION CAUSED BY SAND INGESTION

BY

W. TABAKOFF AND C. BALAN

Supported by:

NATIONAL AERONAUTICS AND SPACE ADMINISTRATION

Lewis Research Center

Grant No. NSG 3218

November 1982

NASA CR 168067

COMPRESSOR CASCADE PERFORMANCE DETERIORATION CAUSED BY SAND INGESTION

by

W. Tabakoff and C. Balan

Department of Aerospace Engineering and Applied Mechanics
University of Cincinnati
Cincinnati, Ohio 45221

Supported by:

NATIONAL AERONAUTICS AND SPACE ADMINISTRATION

Lewis Research Center

Grant No. NSG 3218

November 1982

ORIGINAL PAGE IS
OF POOR QUALITY

1. Report No.	2. Government Accession No.	3. Recipient's Catalog No.
NASA CR 168067		

4. Title and Subtitle	5. Report Date
COMPRESSOR CASCADE PERFORMANCE DETERIORATION CAUSED BY SAND INGESTION	November 1982
	6. Performing Organization Code

7. Author(s)	8. Performing Organization Report No.
W. Tabakoff and C. Balan	
	10. Work Unit No.

9. Performing Organization Name and Address	11. Contract or Grant No.
DEPT. OF AEROSPACE ENGINEERING & APPLIED MECHANICS UNIVERSITY OF CINCINNATI CINCINNATI, OHIO 45221	NSG 3218
	13. Type of Report and Period Covered
	Contractor Report

12. Sponsoring Agency Name and Address	14. Sponsoring Agency Code
NATIONAL AERONAUTICS AND SPACE ADMINISTRATION LEWIS RESEARCH CENTER CLEVELAND, OHIO 44135	

15. Supplementary Notes

Project Manager, Mr. Robert Stubbs, Mail Stop 5-9,
NASA Lewis Research Center, Cleveland, Ohio 44135

16. Abstract

An experimental investigation of airfoil cascade erosion and performance deterioration is conducted in a gas-particle cascade tunnel. The cascade blades are made of 2024 aluminum alloy and the solid particles used are quartz sand. The results of the experimental measurements are presented to show the change in the blade surface erosion, pressure distribution and the total loss coefficient with erosion. The surface quality of the blades exposed to particulate flows are changing the material surfaces. With time, the surface roughness increases and leads to a decrease in engine performance. It was found that the surface roughness values increase asymptotically to a maximum value with increased erosion. The experimental results indicate that the roughness parameters correlate well against the mass of particles impacting unit area of the surface. Such a correlation is useful in aerodynamics and performance computations in turbomachinery.

17. Key Words (Suggested by Author(s))	18. Distribution Statement
Particulate Flow Turbomachinery	Unclassified - unlimited STAR Category 02

19. Security Classif. (of this report)	20. Security Classif. (of this page)	21. No. of Pages	22. Price*
UNCLASSIFIED	UNCLASSIFIED	67	

* For sale by the National Technical Information Service, Springfield, Virginia 22161

NASA-C-168 (Rev. 10-75)

TABLE OF CONTENTS

SUMMARY

An experimental investigation of airfoil cascade erosion and performance deterioration is conducted in a gas-particle cascade tunnel. The cascade blades are made of 6061-T6 Aluminum alloy and the solid particles used are quartz sand. The results of the experimental measurements are presented to show the change in the blade surface erosion, pressure distribution and the total loss coefficient with erosion. The surface quality of the blades exposed to particulate flows are changing the material surfaces. With time, the surface roughness increases and leads to a decrease in engine performance. It was found that the surface roughness values increase asymptotically to a maximum value with increased erosion. The experimental results indicate that the roughness parameters correlate well against the mass of particles impacting unit area of the surface. Such a correlation is useful in aerodynamics and performance computations in turbomachinery.

1. INTRODUCTION

Aircraft engines operating in a polluted environment is of serious concern to the aviation industry due to the performance deterioration in terms of expensive short overhaul periods and costly fuel bills. One of the many factors, leading to a deterioration of performance with time, is sand ingestion.

The ingested sand causes serious damage to the engine by eroding the rotor and stator vanes of the compressor and other engine components. The associated problems can range from blade aerodynamic changes, excessive vibration due to inbalance in the rotating components, mechanical failure of the compressor vanes and possible thermal failure of the turbine components (blocking of the cooling holes, etc.). Such mechanical problems can lead to a total engine failure. The changes in the airfoil sections profile and the increased blade surface roughness due to erosion can cause significant changes of the aerodynamic characteristics of the compressor and turbine leading to an overall decrease in engine performance.

In order to understand the blade erosion and the performance changes, tests were conducted on a specially built cascade erosion tunnel. The blade profiles used were NACA 65 series airfoil sections and the blades were made of 6061-T6 Aluminum. The cascade performance was monitored at different degrees of erosion.

Based on the experimental results, it was decided, that it is necessary to study the roughness development of the eroded surfaces. Therefore, further tests were conducted on 6061-T6

aluminum alloy flat plates. This was followed up by the design and fabrication of a single stage test compressor for erosion studies. However, funding limitations, did not allow the completion of this study.

2. PERFORMANCE OF ERODED BLADES

The blade erosion damage results in pitting and cutting of the blade leading and trailing edges, and a general increase in the blade surface roughness. The basic material removal mechanism is a complex function of the physical properties of the material being eroded, the particle material, size, impact angle and velocity. This mechanism has been investigated by many researchers and has resulted in experimental correlations for the material removal rate in terms of the erosion parameters [1, 2]. In addition, Tabakoff and his researchers [3] have also studied the inelastic collisions between the particle and the target materials which have lead to statistical, experimental correlations for the restitution coefficients between various particle and target materials. Tabakoff and Hussein [4, 5] formulated the equation of particle motion through a turbomachine and developed a computational model for predicting the trajectories and impact points on the blade surfaces.

Bamert et al. [6, 7, 8] investigated the effect of surface roughness and the effect of manufacturing tolerances of the airfoil shapes on the performance of the turbine and compressor

blade sections, and arrived at a conclusion that the performance does change significantly. Shaffler et al. [9] investigated the effect of surface roughness on the multistage compressor. They found that even the small changes in surface roughness due to the various manufacturing techniques can lead to considerable reduction in the efficiency of the high pressure stages. It is obvious from these findings that the erosion related performance deterioration can be of considerable magnitude.

2.1 The Erosion Tunnel

A special cascade erosion tunnel was built that provides a gas particle flow mixture. A schematic configuration of the tunnel is shown in Fig. 1. It consists of the following components: particle feeder (A), main air supply pipe (B), settling chamber and particle injector (C), accelerating tunnel (D), test section (E), and exhaust tank (F). The equipment functions as follows: a measured amount of abrasive grit of a given constituency is placed into the particle feeder (A). The particles are fed into a secondary air source and blown up to the particle injector in the settling chamber (C), where it mixes with the main air supply (B). The particles are accelerated by the high velocity air in the constant area duct (D), before impacting the cascades in the test section (E). Past the test section the particulate flow is exhausted through exhaust collector (F).

Since the particles are accelerated in the constant area duct by the aerodynamic drag forces, their velocity before

impacting the cascade would depend upon the air velocity, the particle size and the length of the acceleration section (D). Figure 2 gives an illustration of the dynamics of relatively large 165 micron particles with air flow velocity of 130 m/s. From this figure it can be seen that the particles final velocity is an exponential function of the tunnel length. Based on these findings, a tunnel length of 3 meters was used in obtaining the experimental data. The test section (E) is of slightly smaller cross section than the accelerating duct (D). This sudden contraction was provided to remove any low velocity fluid very close to the walls. Any other complex method of boundary layer control was not feasible due to the presence of the particle in the flow field. The test section is of 35.5 mm x 135 mm rectangular cross section. Because of the tunnel dimensions, it was decided to select low aspect ratio and high solidity, in order to have blades with reasonable chord length.

2.2 Instrumentation

The primary and secondary air mass flow rates were measured using standard ASME orifice flow meters. The blade surface pressure distribution, the total pressure in the settling chamber, and the test section wall static pressures were measured using a scanivalve-pressure transducer-digital recorder system. In addition, a multitube manometer bank was used to record the blade surface pressure distribution occasionally.

This provided a check on the accuracy of the scanivalve system of pressure measurement.

The cascade inlet and outlet total pressures and the flow angles were measured using a special wedge probe.

2.3 Cascade Description

The compressor blades chosen for the tests were NACA 65-010 airfoil base profiles superimposed on $C_{\ell,0} = 1.0$ mean line [10]. The blades have a maximum thickness to chord ratio of 10% and a camber angle of 35°. These blades were produced by an extrusion of 6061 aluminum alloy and are of 50.8 mm chord and 37.5 mm height. Three types of cascades were tested in this study; one was an accelerating cascade and the other two were diffusing cascades. The details of the cascade are given in Table I. Ih all the cases, the central blade passage was fitted with 18 surface static pressure probes, whose locations are given in Table II, and shown in Fig. 3.

2.4 Experimental Technique

The first step in this study was to determine the performance of uneroded cascades. The performance test consisted of measuring the blade surface pressure distribution, the inlet and exit total pressure and the flow angle survey. These tests were conducted at an inlet Mach number of 0.15. The blade chord Reynolds number was 1.57×10^5. From the total pressure survey the total pressure loss coefficient across the cascade was determined. The initial weight of the uneroded blade was also recorded using a microbalance.

The second step was to erode the cascades by a measured quantity of 165 microns mean diameter quartz sand. The sand was introduced in the tunnel at a predetermined rate, and the concentration of the sand in the tunnel was maintained at 0.015. The concentration α is defined as the mass of sand per unit mass of air flow through the cascade.

The third step was to measure the performance of the eroded cascades. This was performed exactly the same as the first step. The weight of the blades, the total pressure loss coefficient, the flow angle and the pressure distribution were determined once again. The inlet Mach number was maintained at 0.15 during this step.

Steps two and three were repeated until the blades were eroded to a point, beyond which no useful information was expected.

2.5 Results and Discussion

From the erosion damage of the airfoil cascades, there are two main consequences. The first one is the change in the airfoil geometry and the quality of the surface. This is measured by the quantity of the material removed and the changes in the airfoil dimensions and the increase in the blade surfaces roughness. The second aspect is the change in the flow field due to the change in the airfoil geometry and the surface quality. This is measured by the changes in the pressure distribution and the total pressure loss coefficient of the cascade.

One of the basic problems associated with any multi-parameter system is the proper choice of a single parameter, which can be used to correlate the results. For erosion studies, the most basic parameters are the particle concentration, α, the time of the cascade exposure to the particulate flow, t, the ratio of particle to air velocity, and the dimensions of the cascade. The material removed is a strong function of the mass of particles impacting the blade surfaces. Hence, the parameter, $\dot{M}_{ts}$, defined as the total amount of particle that has passed through unit cascade inlet area at time t, is chosen as the basic parameter for erosion. If the particle concentration, α, and the flow properties at the inlet are known, one can easily compute the cumulative sand mass flow parameter $\dot{M}_{ts}$ as

$$\dot{M}_{ts} = \alpha_m \, t \, \rho_{g_i} \, u_{g_i}$$

where ρ_{g_i} and u_{g_i} are the density and the axial velocity of the fluid at cascade inlet. With the cascade dimensions known, the total amount of sand Q that has passed through a single cascade passage is given as:

$$Q = \dot{M}_{ts} \, h \, S$$

where h and S are the blade height and spacing of the cascade.

Blade Erosion Rate

Figure 4 shows the weight loss of the three cascades as a function of the cumulative mass flow parameter. All the tests were carried out at a mean particle concentration α_m of 0.015. It can be seen from this figure that the weight loss is slightly nonlinear during the early period and then it becomes essentially linear during the later periods.

As mentioned earlier, the material removal is a complex function of the local angle of attack of the particles, the impacting particle velocities and particle sizes. Since the angle of attack of the particles continuously change along the airfoil surfaces, the observed erosion is a combination of all the local material removal rates. Figure 5 shows the measured weight loss of flat plate specimens as a function of time taken from reference [11]. It can be observed from this figure that there is a small incubation period, during which even a slight weight increase is possible. This increase in the weight of the specimen during the early periods is attributed to the solid particle embedment. The observed weight loss can be considered linear. Based on the results, the weight loss of these blades in cascade can be expressed in terms of overall material removal rate which may be expressed in gm/kg computed as follows:

$$\varepsilon_o = \Delta W/Q$$

where ΔW is the blade weight loss. Table 3 gives the overall

material removal rate for the three cascades. It is quite apparent that the weight loss is a strong function of the stagger. The IGV cascade shows a lower material removal rate as compared to the diffusing cascades. In all the cases the material removed from the cascades was about 5 percent of the initial weight. Also, the decrease in the blade chord was about 1.6 percent.

In addition the following observations may be made regarding the blade erosion, referring to Figs. 6 and 7.

1. The erosion of the blade leading edges were similar in all the cases. There was an erosion step formation on both the suction and the pressure blade sides. The blade leading edges were flattened and rougher.
2. The erosion on the pressure side of the accelerating cascade, was severe downstream from the leading edge. The surface roughness increased towards the trailing edge. In addition the blade trailing edge became very thin.
3. The erosion on the pressure side of the diffusing cascade was much higher in the region immediately following the leading edge and it became significantly lower near the trailing edge region.
4. In all the cases, the blade suction surface remained unaffected for most of the experiments, except for the step formation at the leading edge and the increased surface roughness of a small region immediately following the leading edge.

Blade Surface Pressure Distribution

The test results show that the blade pressure distribution is affected by the presence of erosion. The surface pressure distribution of the cascades is presented in terms of non-dimensional pressure coefficient, C_p, which is defined as:

$$C_p = \frac{P_{t_i} - P_s}{q_i} = \frac{P_{t_i} - P_s}{\frac{1}{2}\rho_i V_i^2} \qquad (1)$$

where P_{t_i} is the inlet total pressure, P_s the local surface static pressure, V_i, the inlet gas velocity, and q_i the inlet dynamic head.

Figures 8, 9 and 10 show the surface pressure distribution of the three cascades investigated. It can be seen from these figures that the pressure distribution of cascade II indicates that the cascade should have operated at a fairly high positive incidence angle. Later, an investigation of the eroded cascade and the tunnel test section proved that this was true. The severe erosion of the tunnel test section, compounded by a mistake in the stagger setting of this particular cascade has led to this problem. This problem was later specified in the testing of the third cascade.

The pressure distribution of the eroded cascades were recorded as measured at the time when the testing of the particular cascade was discontinued. An inspection of these figures show that in all the cases, the pressure distribution is altered in such a way that the blade loading decreases with erosion. The blade loading is represented by the area between

the suction and pressure side curves. In all the cases, the exit angle did not change by more than one degree and hence the change in the blade loading probably is not as high as indicated by the pressure distribution. In addition, it can be observed from Figs. 8, 9 and 10 that the suction side pressure distribution indicates a uniform decrease in the pressure coefficient. The uniform decrease of the pressure coefficient indicates a corresponding decrease in the suction surface velocities. The blade pressure side surface pressure coefficient is not altered for most part of the profile except for a region near the trailing edge.

As mentioned earlier, most of the material removal occurs at the blade pressure surface. Neglecting any variation in the pressure side local surface angles, one can assume the material removal to be uniformly distributed on the entire surface. Under this assumption one can calculate the movement of the pressure surface towards the suction surface. Referring to Fig. 11, for the total material removed, this movement is approximately 0.2 mm. This corresponds to a 4% decrease in the maximum thickness to chord ratio, and an increase in the overall flow passage width. For this reason, the observed decrease in the suction surface velocities are reasonable.

Loss Coefficient

The cascade performance is estimated by the total pressure loss across the cascade. The total pressure loss coefficient ζ can be calculated based on the wake measurements. From the

total pressure traverse data, the loss coefficient was calculated by the following equation:

$$\zeta = \frac{\int_0^S (P_{t_i} - P_{t_e})dy}{S\, q_i} \qquad (2)$$

where S is the blade spacing.

Figure 12 shows the variation of the loss coefficient with the cumulative sand mass flow rate through the cascade. It can be observed from this figure that the trend is the same for all the cases tested. From Fig. 12, it can be seen that there are three distinctive regions (A, B and C). In the first region A, the total pressure loss coefficient of the eroded blades increase steeply by about 50 percent of the uneroded blade value. This is followed by region B where there is only a small increase in the loss coefficient with further erosion, and in region C the loss coefficient suddenly increases very steeply once again.

It can be seen from these figures that the total pressure loss coefficients are much higher for eroded blade than normally reported in any two dimensional cascade tests data. In this investigation the aspect ratio was low (0.50) and this was leading to considerable secondary flow losses in the cascades. Such closely spaced blades usually produce high profile losses and the low aspect ratio blades generates considerable secondary flow losses, consequently the overall loss coefficients are very high. The limitations of the wind tunnel cross section

did not permit testing with high aspect ratio blading. In the absence of any information on the variation of the secondary flow losses with eroded blades, the curves of Fig. 12 represent the overall behavior of the total pressure loss coefficient with varying degrees of erosion.

Based on the test observations, the steep rise in the loss coefficient during the early periods is due to the boundary layer transition. Under normal situations, the transition from laminar to turbulent boundary layers probably occurs somewhere around 0.4 to 0.6 chord. However, a significant increase in the roughness of the leading edge region can cause very early transition leading to a high loss coefficient.

From the data available in the literature [9], the definition for "smooth surface" is defined as any surface can be considered hydraulically smooth if the roughness Reynolds number, Re_{R_p}, is less than 90. The Reynolds number is defined as VR_p/ν, where R_p is the height of the roughness element, and u and ν are the velocity and kinematic viscosity, respectively. From the Reynolds number definition, it can be seen that it needs only small roughness change; for example, a roughness height of 30 microns will make the surface rough. It is quite possible that even smaller roughness heights are enough to make the flow turbulent and possibly starting from the eroded blade leading edge. In the second region B, the loss coefficient increases slightly with erosion. This region represents the increase in the losses due to the increase in

the surface roughness and the changes in the blade profile. At the same time, it should be noted that the increase in the loss coefficient is not very high in this region. This is probably due to the entire increase in roughness being limited to the blade pressure surface only. In the third region C, the loss coefficient increases steeply once again. This is probably due to the flow separation in one or both blade surfaces. Such flow separation is quite possible, since the leading edge and the pressure surface deteriorates continuously leading to considerable local abrupt changes of the airfoil profile.

3. EROSION AND SURFACE QUALITY

The surface quality as well as the erosion rate are dependent on the basic mechanism of erosion. Many theories have been proposed, which range from cutting [12], plowing [13, 14], or local melting [15]. The cutting theory accounts for the material removed as chips equal to the swept volume of the individual impacting particles. The plowing theory explains the plastic deformation and pile-up of material at the exit side of the impact craters, to form limps. Material removal is accomplished by the brittle fracture of these work hardened lips, by subsequent impact of other particles. In reality, the erosion mechanism is a combination of the cutting and plowing actions and possible occasional melting.

These theories are only in their infant stage; they can offer qualitative explanation only on various aspects of erosion. They cannot be used for quantitative estimation of the erosion or surface quality. The present state of the art is such that one still depends on empirical correlations for the prediction of erosion rates. To the date however, no research of significant contribution has been carried out to quantify the change in surface quality of the change in surface quality of the eroded surface. Finnie et al. [16] observed severe ripple formation on sand blasted ductile solids and carried out some theoretical analysis. They concluded that the ripple wavelength should be of the order of particle diameter and that the ripple height grows with prolonged exposure to erosive environment. Several years later the follow-up work on copper material was reported by Carter et al. [17]. Though their report confirmed the findings of Finnie et al., they found that the ripple heights were a minimum around the maximum erosion angle. These data are not useful for the purposes of our interest in turbomachinery since the material investigated was copper.

In the absence of the needed quantitative measurements on the surface roughness of the eroded specimens, tests were conducted on 6061-T6 flat plate specimens. These series of experiments were conducted using silica sand of 165 and 225 microns mean diameter and particle velocity of 100 m/s.

$$(R_s)^2 = \frac{1}{\ell} \int_0^{\ell} y^2 \, dx \qquad (3)$$

where ℓ is the length of the surface trace.

The above equations were used in computing the R_a and R_s values of the eroded surfaces. The R_p values were computed as the difference between the mean heights of the peaks and valleys. The surface roughness definitions are shown in Fig. 13.

In order to arrive at a more reasonable conclusion on the above values, Fast Fourier Transformation of the surface traces were taken, which confirmed the computed λ values. Though there is no definite wave pattern at 90° angle of attack, there are definitely peaks and depressions which are taller or deeper than the R_s values. These values, averaged over the length of the specimen were used in computing the R_p values for the 90° angle of attack.

3.1 Results and Discussion

One of the basic parameters that controls the roughness growth on the impacted surface is the total mass or number of particles impacting on unit area of the surface. In most of the reported works, attempts are made to correlate the data against the time of exposure to a uniform particle flux. In this report, an effort is made to present the results as a function of both the time of exposure, t in min., as well as, the total mass of particles impacting the surface per unit area $\dot{m}_{ts}$ in gm/cm^2.

Figures 14a-14d are the micrographs of the eroded specimens at various angles of attack. All these specimens have been impacted by 124 gms of particles per square cm of the sample surface area. It can be observed from these figures, that the ripple pattern is present up to about 50° angle of attack. Figures 15a-15d represent the surface topography at a fixed angle of attack for different amounts of particles impacting the specimen. These figures explain the development of the well defined ripple structure with increasing amount of the impacting particles. At very small quantities of particles impacting the specimen, the surface is randomly rough, due to the cutting and plowing tracks. As the amount of particles increases, the craters join together to form a well defined ripple pattern. By further increasing the amount of particles, results in the growth of the ripples amplitude. In addition, the general quality of the surface decreases with increased erosion.

The quantification of the parameters associated with the roughness and the ripple structure can be achieved through the centerline average, R_a, root mean square, R_s, and peak to valley heights, R_p, as well as the wave length, λ, of the ripple structure. Typical dek tak profilometer surface traces are shown in Figs. 16a and 16b. Figure 16a represents the surface topography at lower magnification of the x axis and Fig. 16b represents the same at a higher magnification of the x axis. For computational purposes, the higher magnification surface traces were used.

Figures 17a-17e represent the surface traces at various levels of erosion. These traces clearly indicate the increase in the surface roughness as well as the increase in the wavelength of the roughness structure with erosion. The traces shown in Figs. 18a-18g show the changes in the roughness structure with angle of attack for the same amount of particle impact on the unit area of the eroded surface. From these traces the R_a, R_s and R_p values of the roughness elements and the wave length λ of the ripple structure were computed. A plot of the wave length λ as a function of the time of exposure for various angles of attack for 225 microns is given in Fig. 19. It can be seen that the wavelength increases with increasing the angle of attack, α, and it reaches a steady state value with time. When the same results are plotted against the total mass of particle impacting on unit sample area, there is a considerable difference in the nature of the curves, as shown in Fig. 20. These curves are almost parallel to each other. The highest value of λ occurs around 60°. The ripple structure is smaller for lower angles. However, the maximum spread in the wavelengths is only about 30 microns, i.e. about 15 percent of the particle size.

The values of the surface roughness, R_s, for various angles of attack as a function of the total mass of particles impacting unit area of the specimen, are shown in Fig. 21. The inspection of this figure shows that the surface roughness rapidly reaches near steady state values for very low (10°) and very high (60° to 90°) angles of attack. On the other hand, the roughness

values, R_s, are much higher for the angles of attack between 20 to 45 degrees. In addition, one can observe that even at these angles, the roughness values show a tendancy to stabilize to a steady state. Figure 22 shows a plot of the peak to valley heights as a function of the impacting particle mass. The peak to valley heights follow the same trend as the R_s values.

The plot of the R_p as a function of time for various angles of attack is shown in Fig. 23. These curves exhibit different characteristics, for example at 60° and 90° angles of attack. R_p raise very steeply to their steady state values and then remain constant with time. They intersect the other curves except the curve for 10° angle of attack. Figure 24 represents the peak to valley heights that are cross plotted against the angle of attack for various durations of exposure. From this figure, it can be seen that, for very small exposure times, the curves indicate an apparent minimum around 45° to 50° angles of attack. For fairly large durations of exposure, the R_p values show an entirely different tendency. All the curves show a maximum R_p value around 30°. The only comparable experimental results are discussed by Carter et al. [16] for copper surfaces. They observed only a local minimum around 40° but not the change in the nature of these curves as in the present case. It is probable that they have not reached steady state conditions with the roughness amplitude values in their experiments.

In all the cases tested, it was found that there is a definite relation between the R_s, R_a values and the peak to valley heights, R_p. The relations $R_p = 2.5\ R_s$ and $R_p = 3.1\ R_a$ are valid at all angles of attack and different amounts of erosion within 5% accuracy.

In order to get a better understanding of the roughness formation, the values of R_p were plotted in nondimensional form versus the total mass of particle impacting per unit area for two particle sizes as shown in Fig. 25. From the inspection of this figure, one can see that the experimental points fall closely on the same curves, for 165 and 225 micron particles. The trend observed indicates that there is a definite asymptotic maximum on the roughness heights with the total mass of particles impacting unit area of the specimen.

Figure 26 shows a plot of the nondimensional roughness heights as a function of the angle of attack for various mass of particles impacting unit area of the specimen. The maximum roughness height occurred around 30° angle of attack and the roughness height is approximately slightly less than 0.2 times the particle diameter. The definite relation between the R_a, R_s and R_p values indicate that there is a good correlation between the various types of surface roughness and some erosion parameters such as angle of attack, the mass of particles impacting the specimen, and particle diameter. However, further investigations are needed on the effect of particle velocities and particle sizes before an empirical correlation is attempted.

4. CONCLUSIONS

Based on the experiments conducted on NACA 65(10)10 airfoil cascades, it was found that the performance changes considerably with the erosion. The results are correlated against a single parameter, $\dot{M}_{ts}$ (total cumulative mass flow parameter). The weight loss of the blades changes significantly with the stagger angles. The cascade with the negative stagger angle, simulating the inlet guide vanes produced the least erosion, while the highly diffusing cascade with higher positive stagger angle produced the highest erosion. In all the cases tested, the pressure surfaces and the leading edges were severely eroded. The high volume of material removed on the pressure surface leads to an increase in the overall channel dimensions. The consequent decrease in the surface velocities is clearly demonstrated by the changes in the suction surface pressure coefficients. In all the cases investigated, the decrease in the blade chord was about 2 percent and the change in the exit flow angle was less than 1 degree.

The performance of the cascades indicate that the total pressure loss coefficient increases by about 50 percent during the early period of erosion. This is probably due to the erosion of the blade leading edge and subsequent changes in the boundary layer transition. Further erosion of the cascades is associated with a slight increase in the loss coefficient. This can be attributed to the increased blade pressure surface roughness with increasing erosion. With continued erosion, the loss

coefficient suddenly increases at a rapid rate. This indicates that considerable separation of the boundary layer occurs associated with the changes in the blade profiles due to erosion.

Further tests were conducted on aluminum flat plate samples, to study the roughness mechanism. It was found that the surface roughness values increase asymptotically to a maximum value with increased erosion. The maximum roughness value of about 0.2 times the particle diameter occurs around 30 degree angle of attack. In the absence of any quantitative theoretical models, as in the case of erosion rate prediction, it is necessary to use empirical correlations for the prediction of the surface roughness. The experimental results indicate that the roughness parameters correlate well against the mass of particles impacting unit area of the surface. However, further experiments are needed before any correlation can be attempted. Such a correlation will be very useful in aerodynamics and performance computations for turbomachinery.

REFERENCES

1. Grant, G., and Tabakoff, W., "Erosion Prediction in Turbomacninery Resulting from Environmental Solid Particles," Journal of Aircraft, Vol. 12, No. 5, May 1975, pp. 471-478.
2. Tabakoff, W., Kotwal, R. and Hamed, A., "Erosion Study of Different Materials Affected by Coal Ash Particles," Wear, 52, 1979, pp. 161-173.
3. Wakeman, T. and Tabakoff, W., "Measured Particle Rebound Characteristics Useful for Erosion Prediction," ASME Paper No. 82-GT-170.
4. Tabakoff, W. and Hussein, M.F., "Trajectories of Particles Suspended in Fluid Flow Through Cascades," Journal of Aircraft, Vol. 8, No. 1, January 1971.
5. Hussein, M.F. and Tabakoff, W., "Dynamic Behavior of Solid Particles Suspended by Polluted Flow in a Turbine Stage." Journal of Aircraft, Vol. 10, No. 7, July 1973.
6. Bammert, K. and Sandstede, H., "Measurements Concerning the Influence of Surface Roughness and Profile Changes on the Performance of Gas Turbines," Journal of Engineering for Power, July 1972, pp. 207-213.
7. Bammert, K., and Sandstede, H., "Measurements of the Boundary Layer Development Along a Turbine Blade with Rough Surfaces." ASME paper No. 80-GT-40.
8. Bammert, K., and Woelk, G.U., "The Influence of the Blading Surface Roughness on the Aerodynamic Behavior and Characteristic of an Axial Compressor." Journal of Engineering for power, April 1980, Vol.102, pp. 283-287.

9. Schaffler, A., "Experimental and Analytical Investigation of the Effects of Reynolds Number and Blade Surface Roughness on Multistage Axial Flow Compressor," Journal of Engineering for Power, January 1980, Vol. 102, pp. 5-13.

10. Emery, J.C., Herrig, L.J., Erwig, J.R. and Felix, A.R., "Systematic Two-dimensional Cascade Tests of NACA-65 Series Compressor Blades at Low Speeds," NACA Report 1368.

11. Ives, L.K., and Ruff, A.W., "Electron Microscopy Study of Erosion Damage in Copper," Erosion Prevention and Useful Applications ASTM Special Publication 664, 1979, pp. 5-35.

12. Finnie, I., "Some Observations on the Erosion of Ductile Materials," Wear, 19, 1972, pp. 81-90.

13. Hutchings, I.M., and Winter, R.E., "Particle Erosion of Ductile Metals: A Mechanism of Material Removal," Wear, 27, 1974, pp. 121-128.

14. Tilly, G.P., "Erosion Caused by Airborne Particles," Wear, 14, 1969, pp. 63-79.

15. Smeltzer, G.E., Gulden, M.E. and Compton, W.A., "Mechanisms of Metal Removal by Impacting Dust Particles," Journal of Basic Engineering, Sept. 1970, pp. 639-646.

16. Finnie, I., and Kabil, Y.H., "On the Formation of Surface Ripples During Erosion," Wear 8, 1965, pp. 60-69.

17. Carter, G., Nobes, M.J., and Arshak, K.I., "The Mechanism of Ripple Generation on Sand Blasted Ductile Solids," Wear, 65, 1980, pp. 151-174.

NOMENCLATURE

C	blade chord, m
C_p	pressure coefficient
h	blade height, m
ℓ	length, m
$\dot{M}_{ts}$	cummulative and mass flow parameter, kg/cm^2
$\dot{m}_{ts}$	total amount of particle impacting unit area, gm/cm^2
$\dot{m}$	mass flow, kg/sec
P	pressure, N/m^2
q	dynamic head, $\frac{1}{2}\rho V^2$, N/m^2
Q	total amount of sand, kg
R_a	arithmetic average roughness, m
R_p	height of roughness elements, m
R_s	root mean square roughness, m
Re_{R_p}	roughness Reynolds number
S	blade spacing, m
t	time, sec
u	axial velocity, m/sec
V	velocity, m/sec
ΔW	weight loss, gm
x,y	coordinate directions
α_m	mass concentration, $\dot{m}_p/\dot{m}_g$
ε_o	overall erosion rate, gm/kg
ξ	total pressure loss coefficient
λ	wave length of ripple structure, m
ρ	density, kg/m^3
ν	kinematic viscosity, m^2/sec

Subscript

ax	axial
e	exit
g	gas
i	inlet
p	particle
s	static
t	total

TABLE I

LOCATION OF SURFACE PRESSURE PROBES

Suction	Pressure	x/C_{ax}
S_1	P_1	0.040
S_2	P_2	0.125
S_3	P_3	0.250
S_4	P_4	0.350
S_5	P_5	0.475
S_6	P_6	0.625
S_7	P_7	0.725
S_8	P_8	0.825
S_9	P_9	0.890

TABLE II

DETAILS OF CASCADES USED IN TESTING PROGRAM

Parameter	Cascade I	Cascade II	Cascade III
Air Inlet Angle, β_1	0.0	35°	45°
Stagger	-20°	+15°	+25°
Camber θ	35°	35°	35°
Incidence	-3.00	-3.00	-3.00
Aspect Ratio	0.75	0.75	0.75
Pitch-Chord Ratio	0.5	0.5	0.5
No. of Blades	6	7	9

ORIGINAL PAGE IS
OF POOR QUALITY

TABLE III

Parameter	Cascade I	Cascade II	Cascade III
ΔW, gm	1.0525	1.0333	1.0165
$\dot{M}_{ts}$, kg/cm^2	0.8000	0.5000	0.4000
Q, kg	7.7419	4.8387	3.871
ε_o, gm/kg	0.13595	0.2135	0.2626
t, min	42	32	29.73

ORIGINAL PAGE IS
OF POOR QUALITY

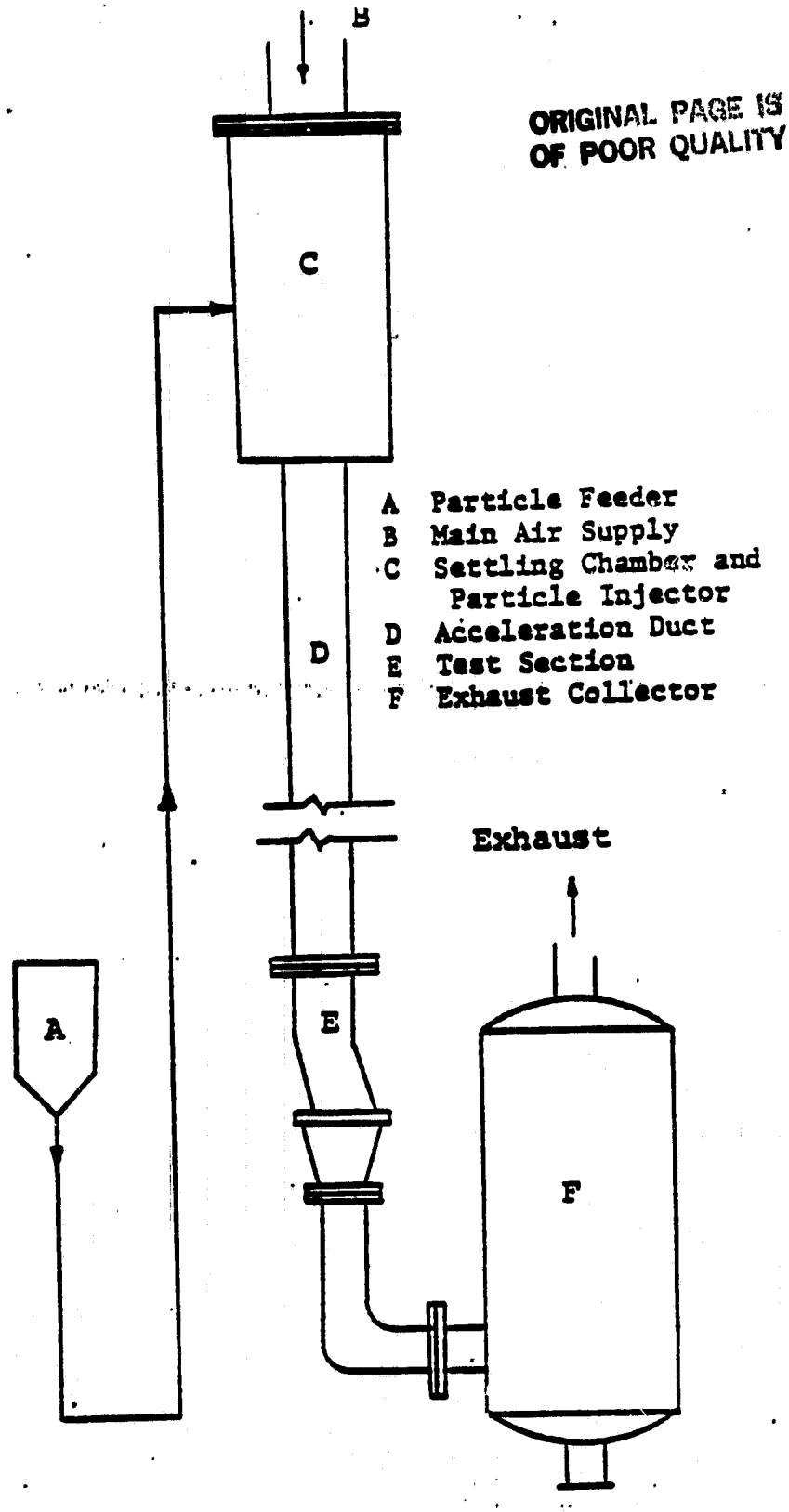

FIG. 1. SCHEMATIC OF CASCADE EROSION TUNNEL.

ORIGINAL PAGE IS
OF POOR QUALITY

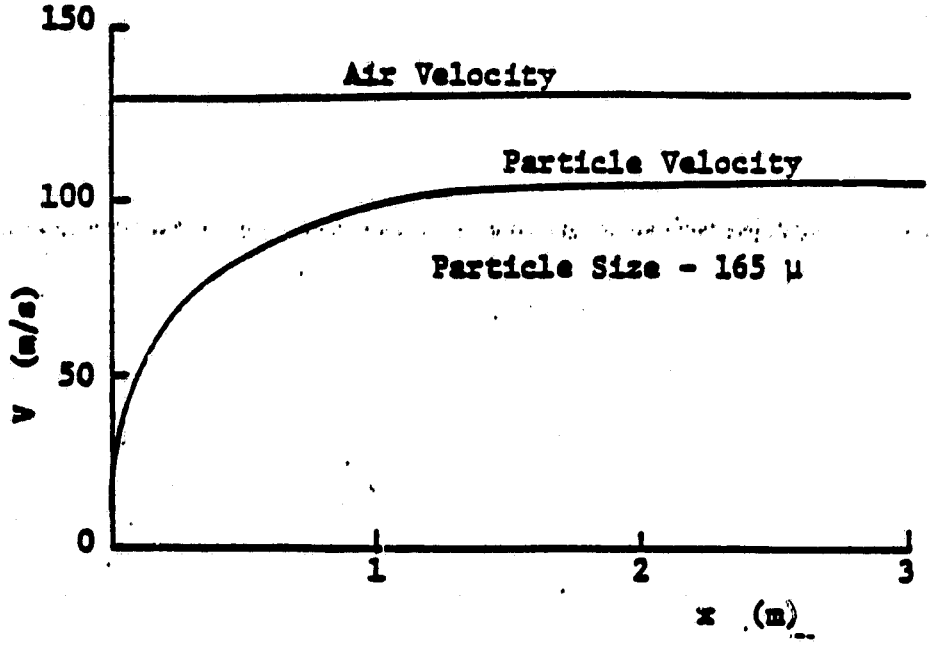

FIG. 2. PARTICLE VELOCITY ALONG THE TUNNEL.

ORIGINAL PAGE IS
OF POOR QUALITY

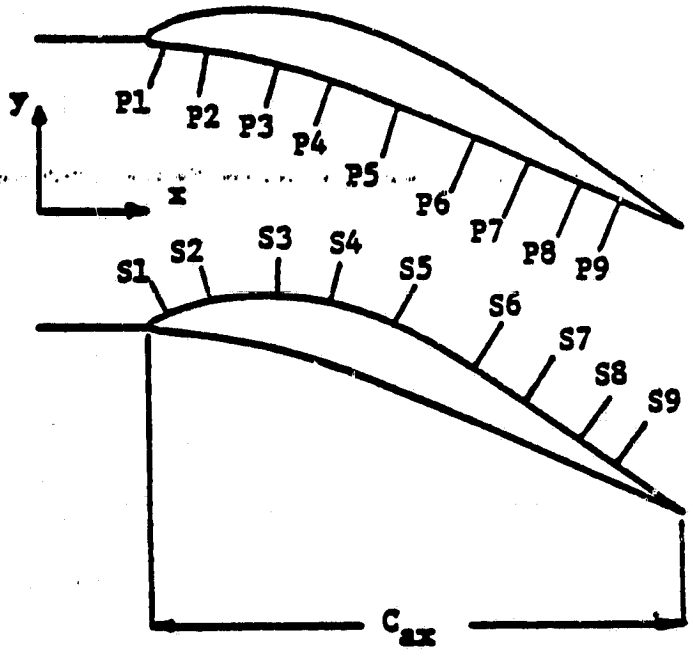

FIG. 3. SCHEMATIC OF PRESSURE TAP LOCATIONS.

ORIGINAL PAGE IS
OF POOR QUALITY

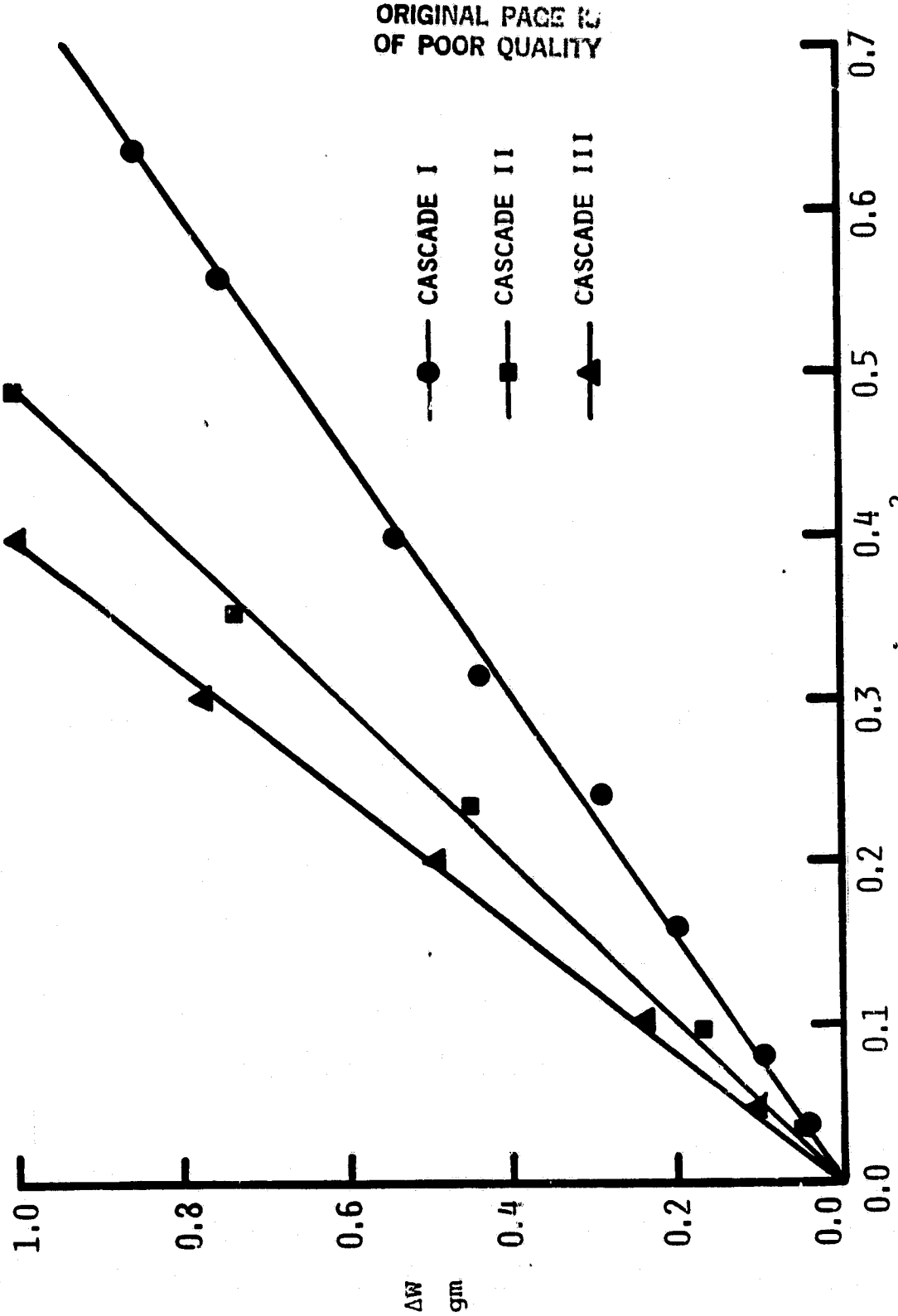

FIG. 4. EXPERIMENTAL WEIGHT LOSS OF THE THREE CASCADES.

ORIGINAL PAGE IS
OF POOR QUALITY

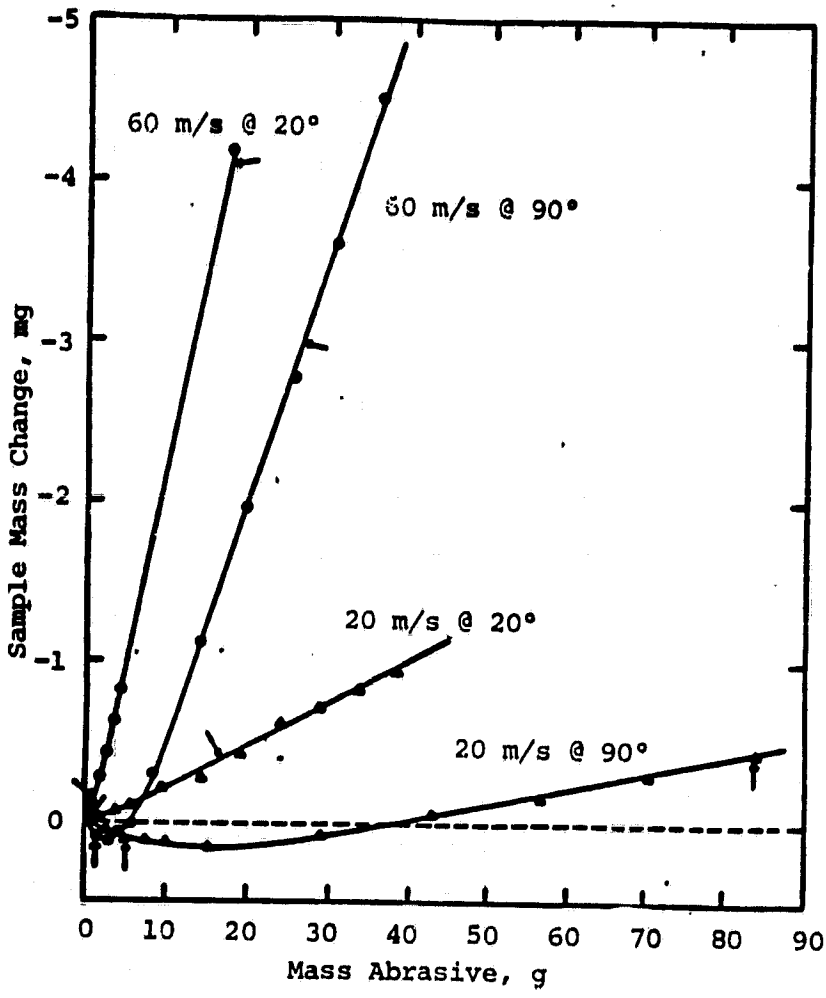

FIG. 5. SAMPLE MASS CHANGE VS. MASS OF PARTICLES (REF. 11).

ORIGINAL PAGE IS
OF POOR QUALITY

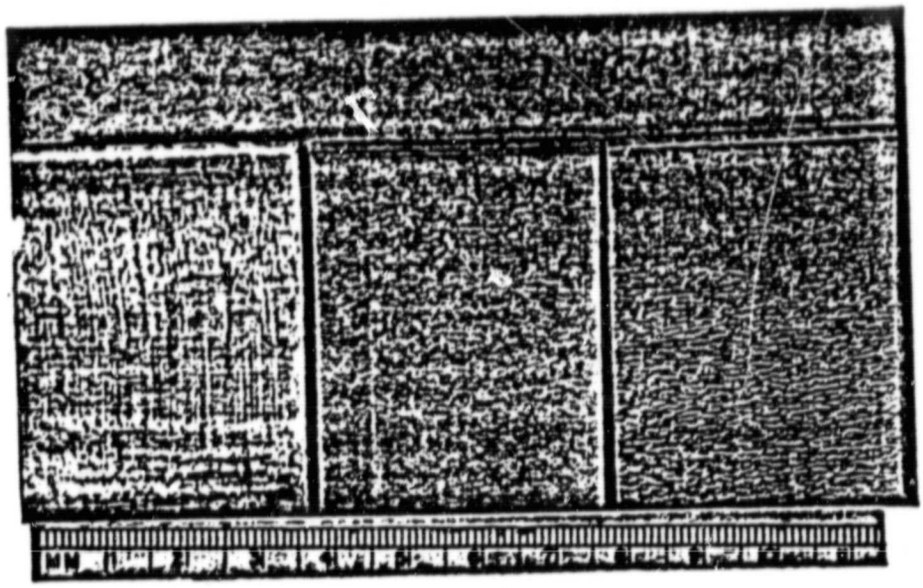

FIG. 6. ERODED BLADE SURFACES.

ORIGINAL PAGE IS
OF POOR QUALITY

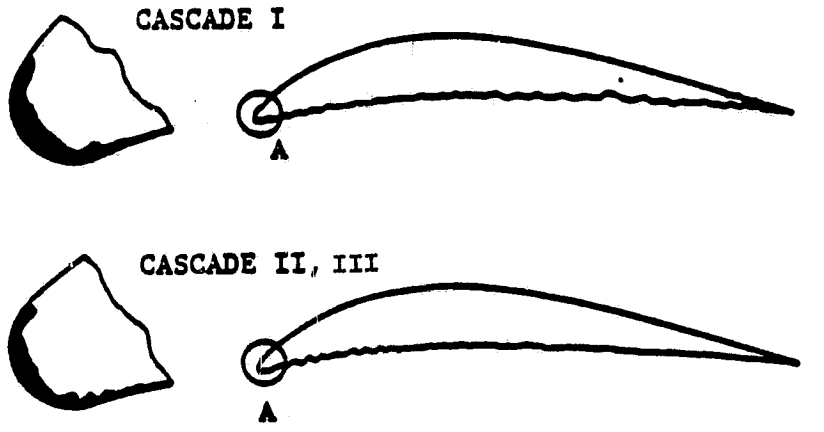

FIG. 7. SCHEMATIC OF EROSION DAMAGE.

ORIGINAL PAGE IS
OF POOR QUALITY

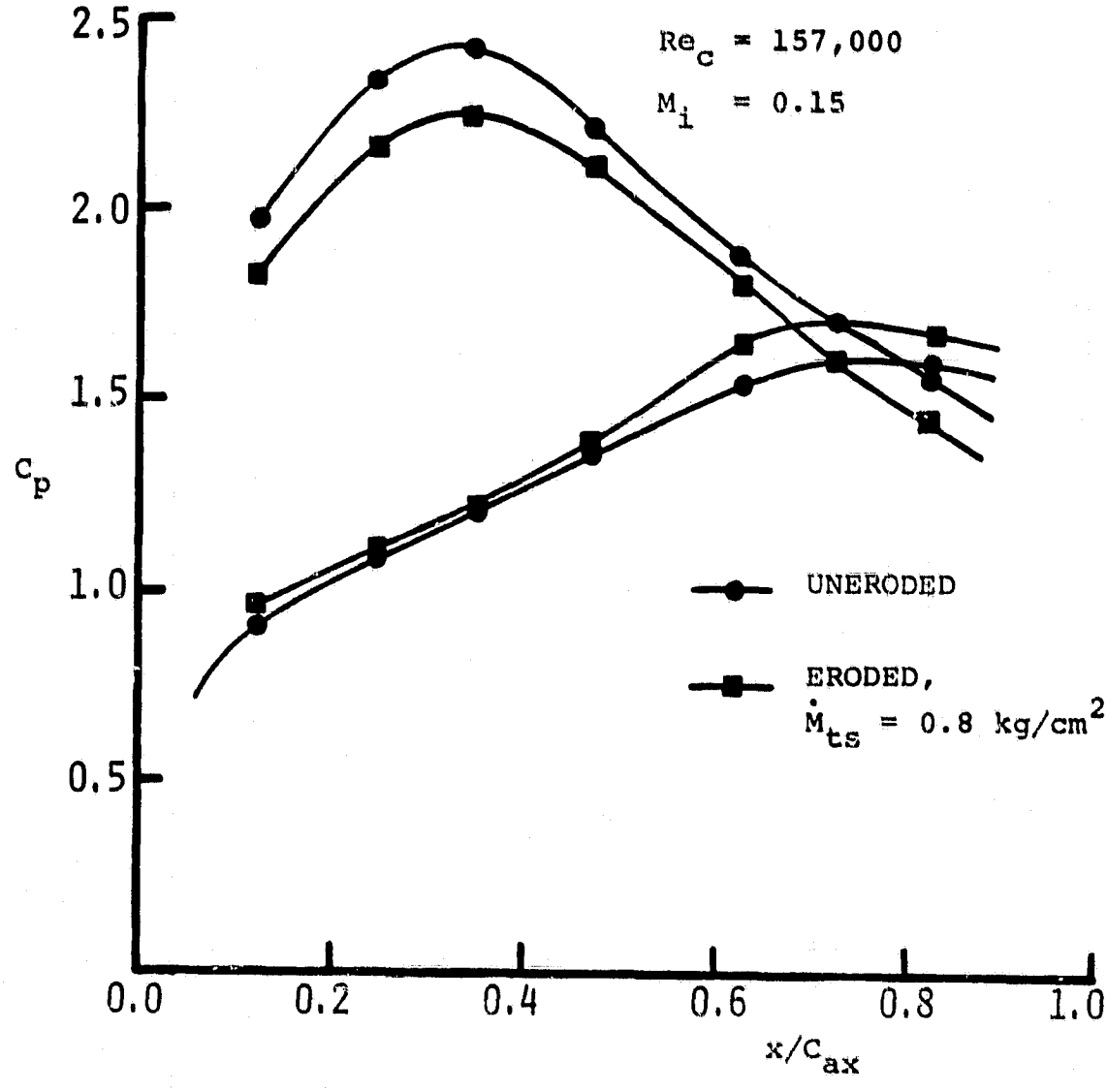

FIG. 8. EXPERIMENTAL PRESSURE DISTRIBUTION OF UNERODED AND ERODED CASCADE I.

ORIGINAL PAGE IS
OF POOR QUALITY

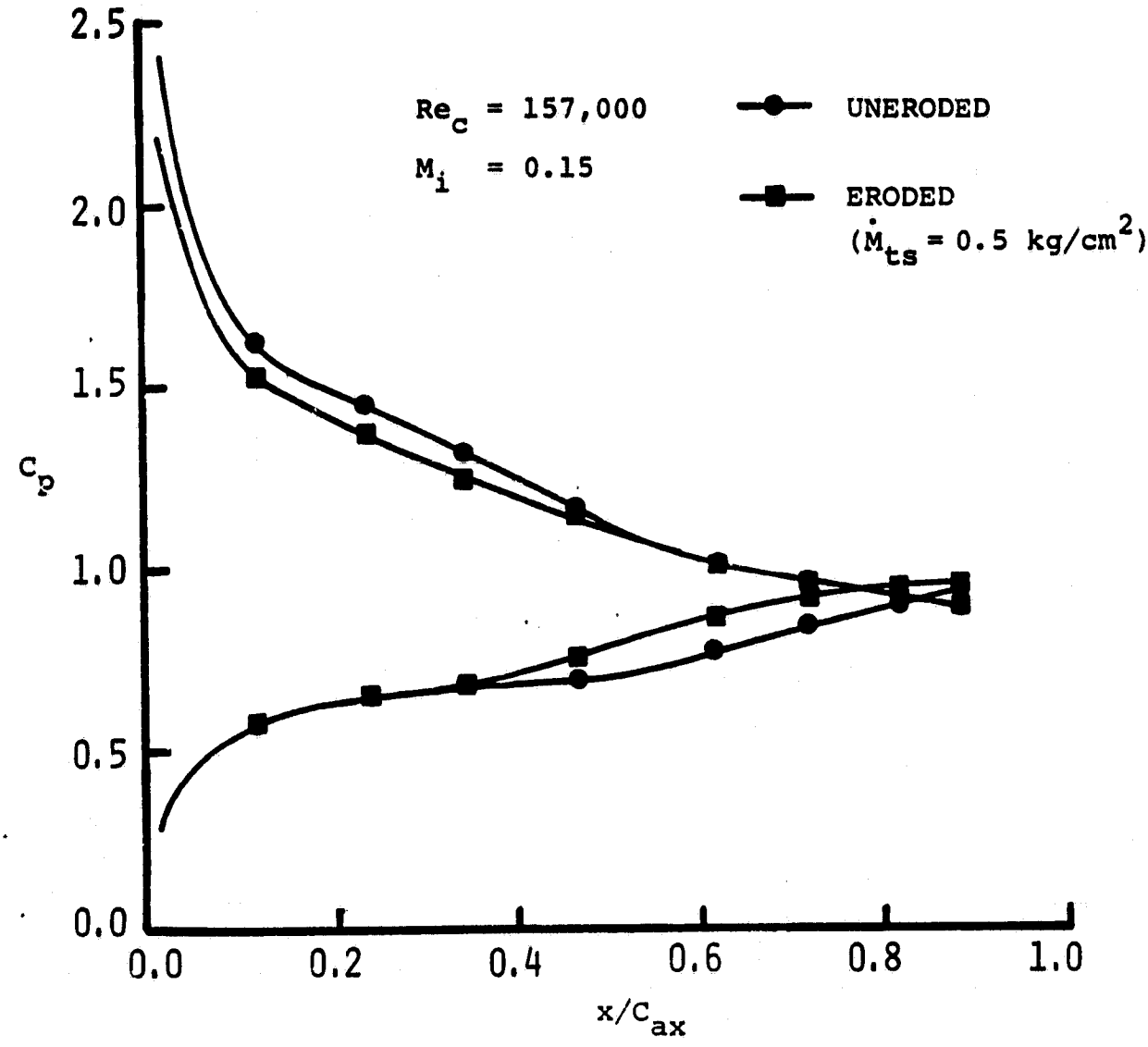

FIG. 9. EXPERIMENTAL PRESSURE DISTRIBUTION OF UNERODED AND ERODED CASCADE II.

ORIGINAL PAGE IS
OF POOR QUALITY

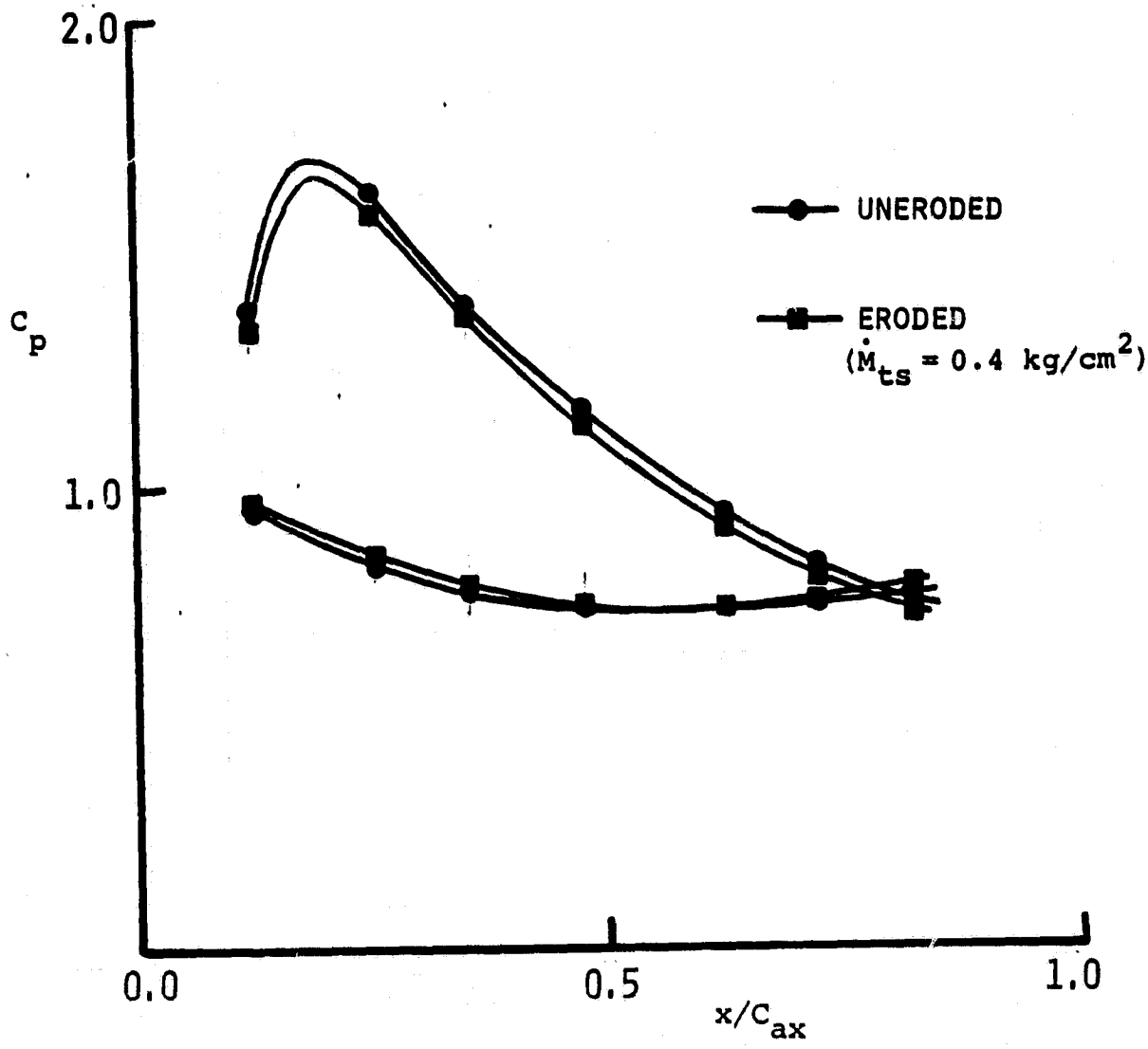

FIG. 10. EXPERIMENTAL PRESSURE DISTRIBUTION OF ERODED AND UNERODED CASCADE III.

ORIGINAL PAGE IS
OF POOR QUALITY

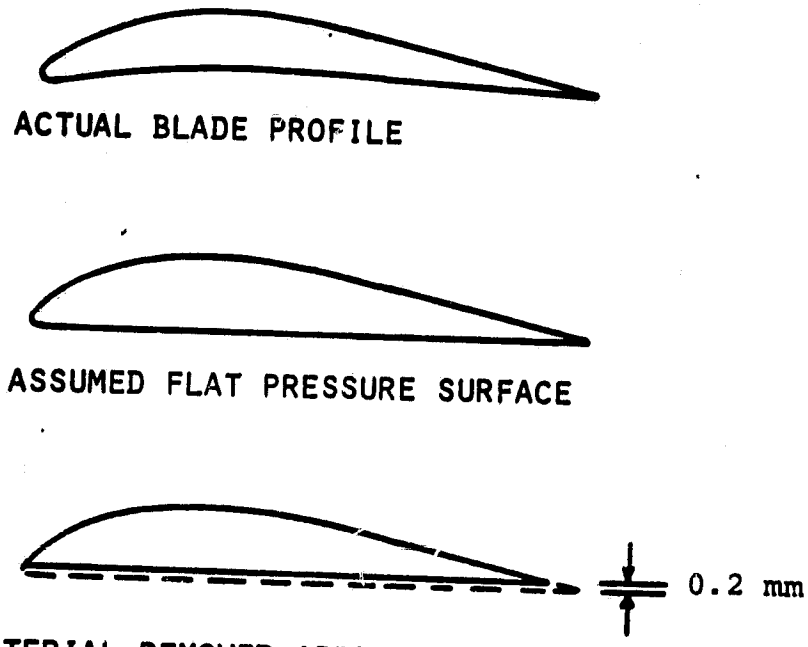

FIG. 11. SCHEMATIC OF APPROXIMATE REDUCTION IN BLADE THICKNESS.

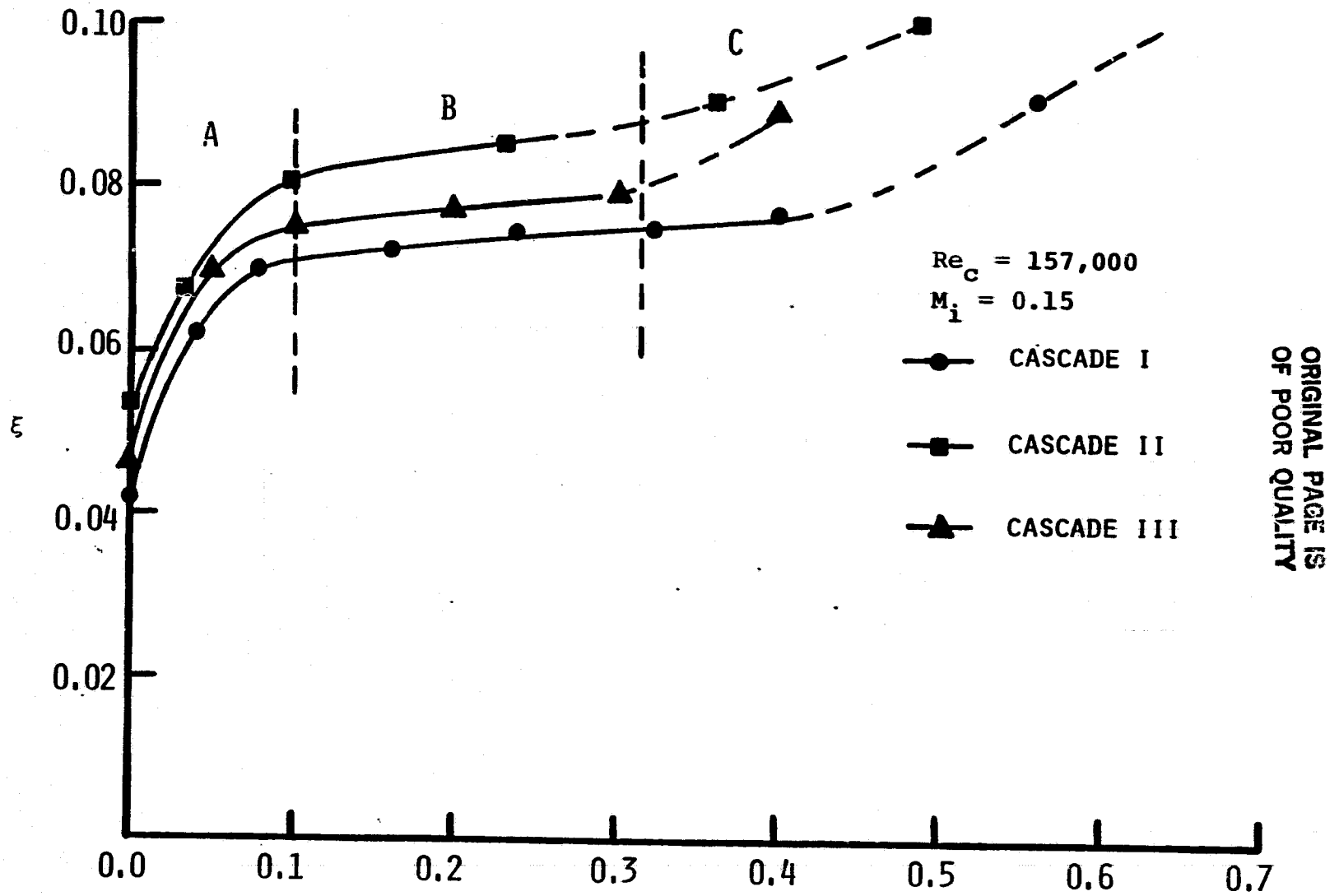

FIG. 12. EXPERIMENTAL LOSS COEFFICIENT OF THE THREE CASCADES AS A FUNCTION OF CUMULATIVE SAND MASS FLOW AT CASCADE INLET.

R_p = MEAN PEAK TO VALLEY HEIGHTS, MICRONS.

R_a = CENTERLINE AVERAGE VALUE, MICRONS.

R_s = ROOT MEAN SQUARE VALUE, MICRONS.

λ = WAVE LENGTH, MICRONS.

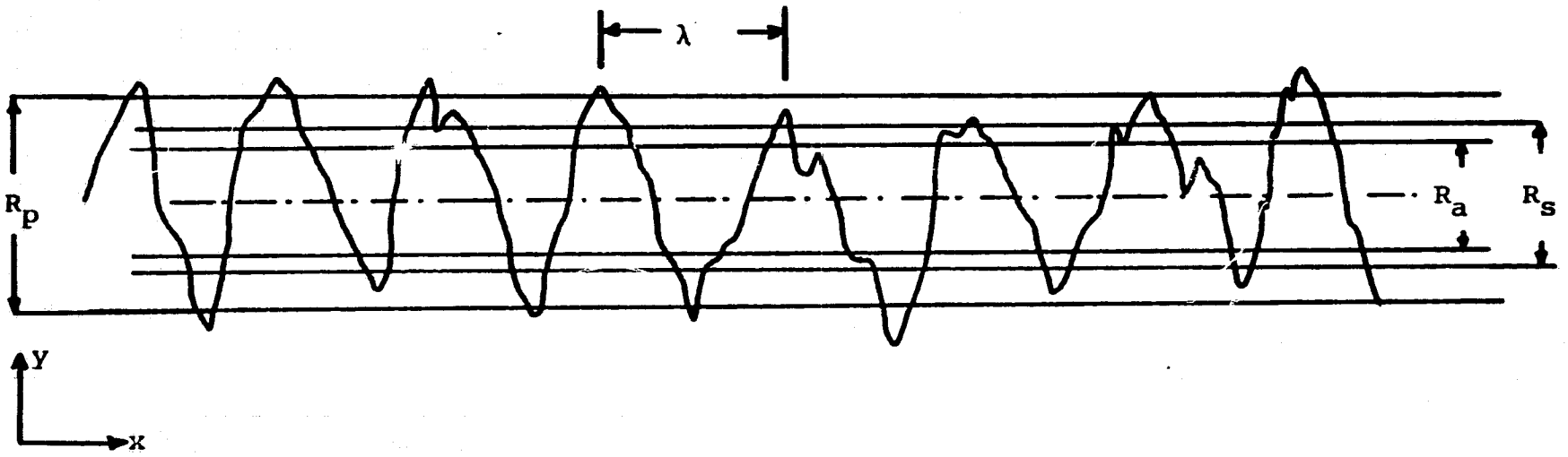

FIG. 13. SURFACE ROUGHNESS DEFINITION.

ORIGINAL PAGE IS
OF POOR QUALITY

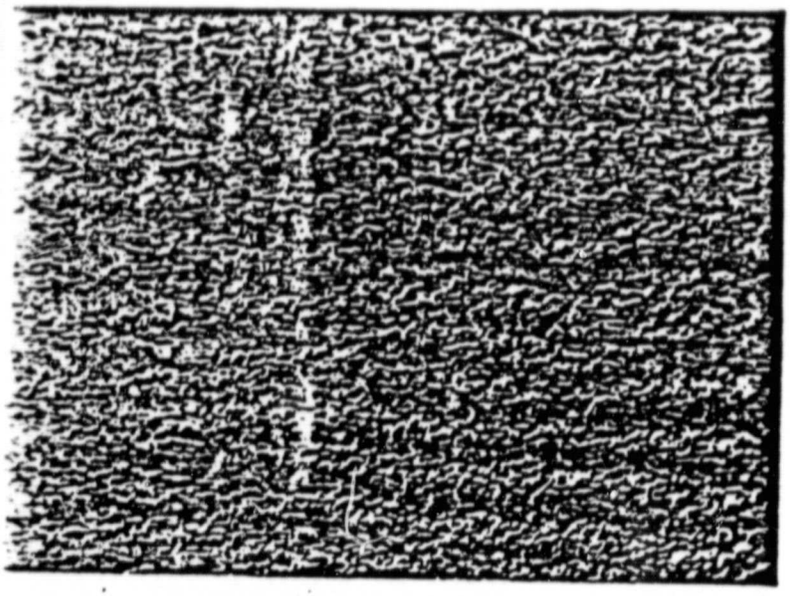

(14A) $\alpha = 20°$
$t = 29.2$ min.

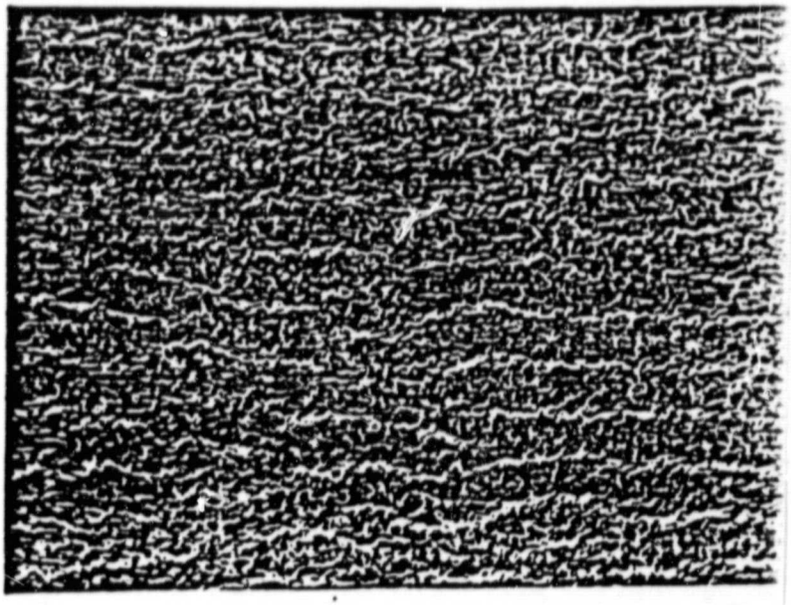

(14C) $\alpha = 45°$
$t = 14.1$ min.

MAGNIFICATION = 20 TIMES

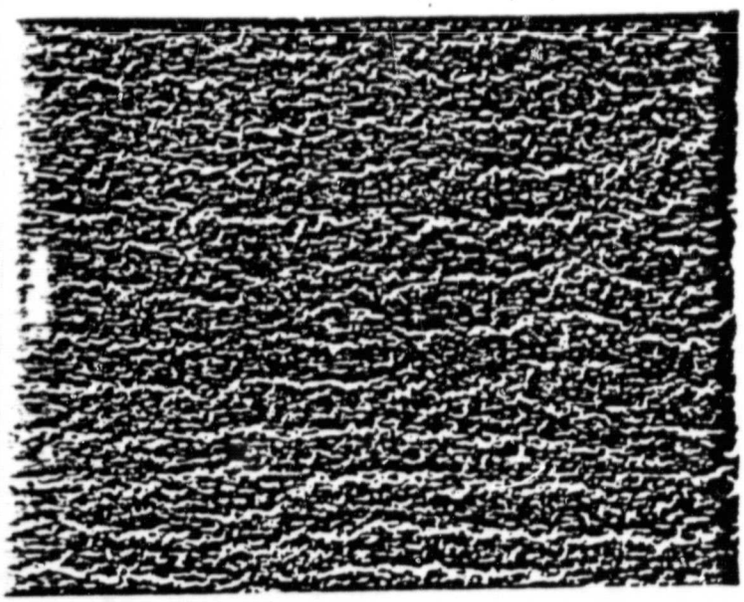

(14B) $\alpha = 30°$
$t = 20$ min.

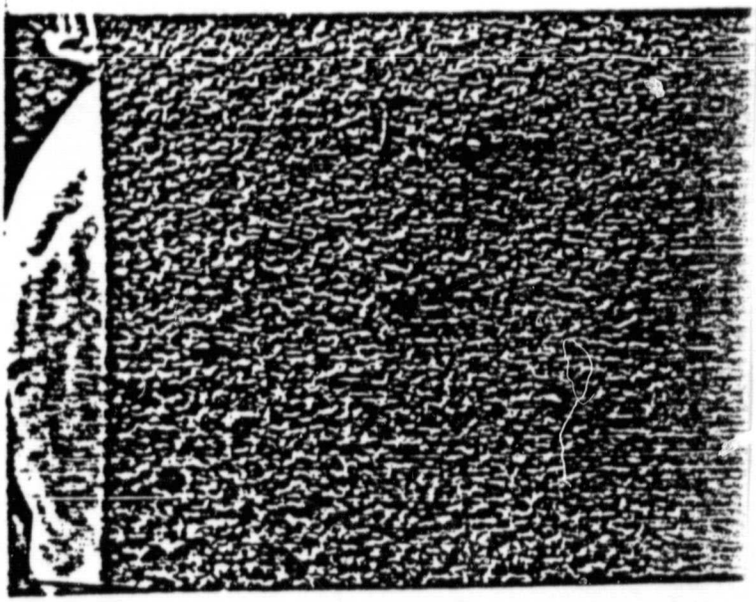

(14D) $\alpha = 60°$
$t = 11.5$ min.

FIG. 14. MICROGRAPHS OF THE ERODED SPECIMENS AT VARIOUS ANGLES OF ATTACK. PARTICLE SIZE = 165 MICRONS.

ORIGINAL PAGE IS
OF POOR QUALITY

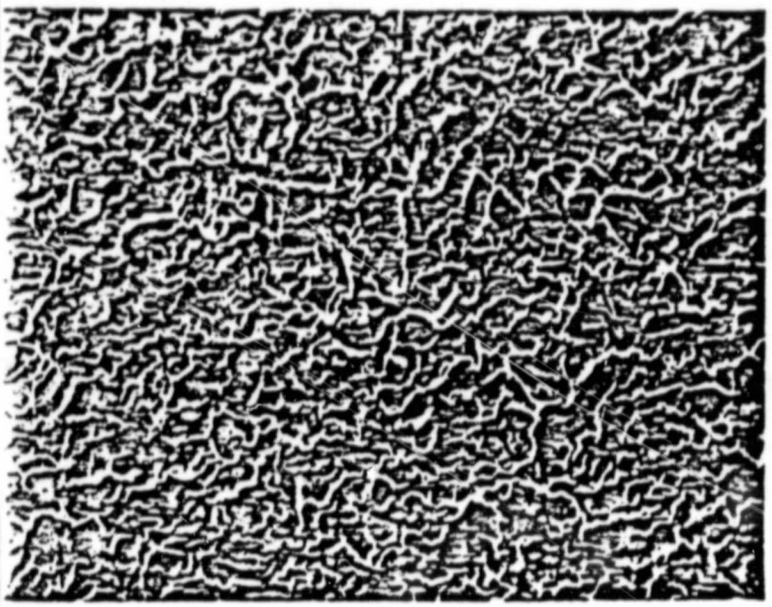

(15A) $\dot{m}_{ts}$ = 3.1 gms/cm^2
t = 0.5 min.

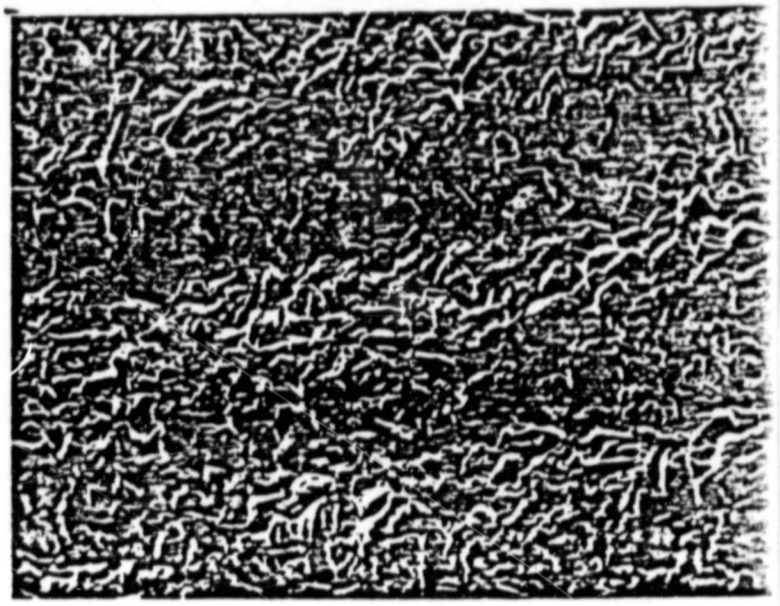

(15C) $\dot{m}_{ts}$ = 62 gms/cm^2
t = 10 min.

MAGNIFICATION = 100 TIMES

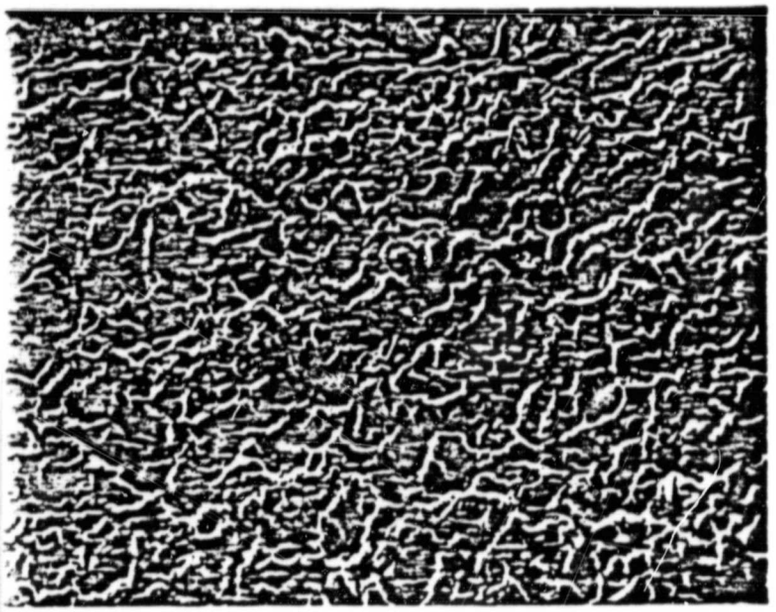

(15B) $\dot{m}_{ts}$ = 12.5 gms/cm^2
t = 2 min.

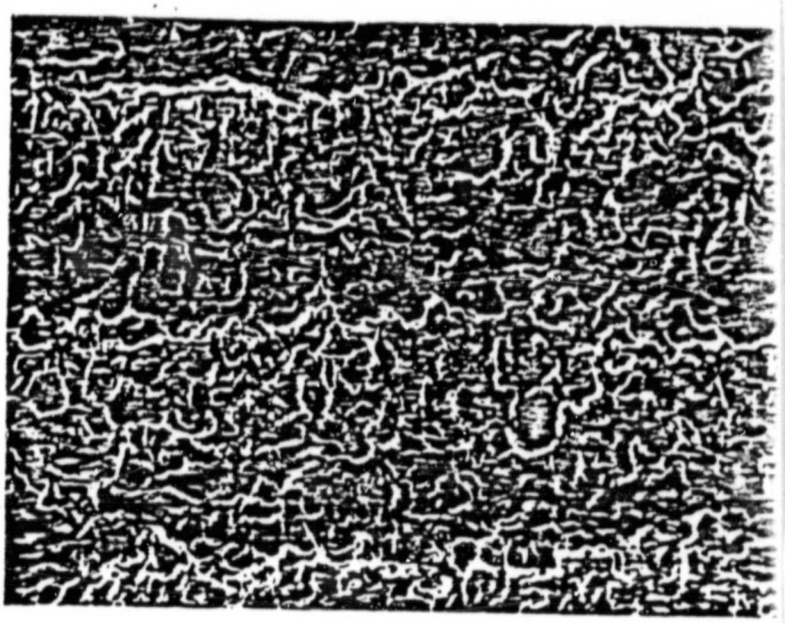

(15D) $\dot{m}_{ts}$ = 124 gms/cm^2
t = 20 min.

FIG. 15. DEVELOPMENT OF RIPPLE FORMATION AT 30^o ANGLE OF ATTACK. PARTICLE SIZE = 165 MICRONS.

ORIGINAL PAGE IS
OF POOR QUALITY

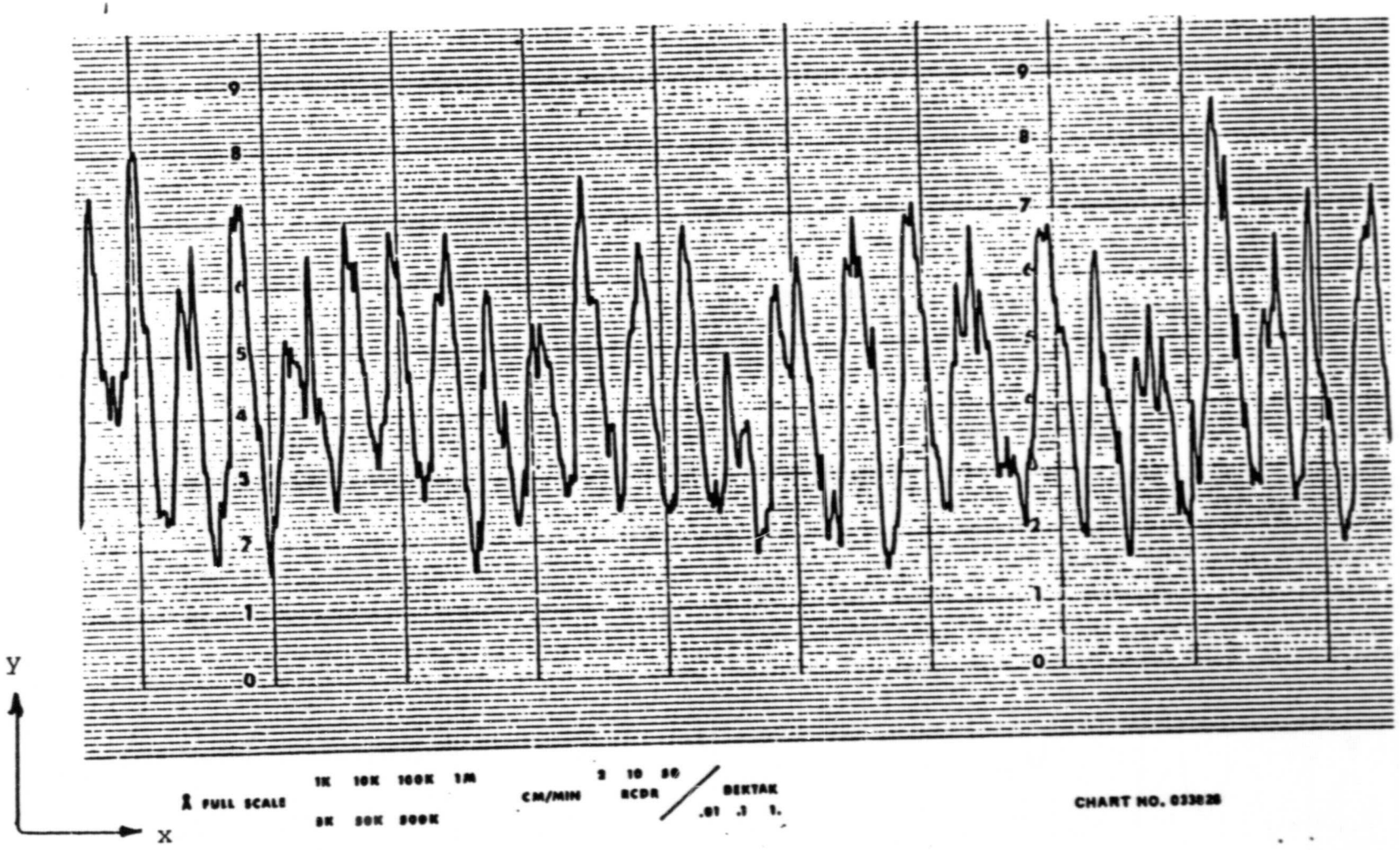

FIG. 16A. TYPICAL SURFACE TRACE OF THE ERODED SURFACE MAGNIFICATION, x = 20 TIMES, y = 1000 TIMES.

ORIGINAL PAGE IS
OF POOR QUALITY

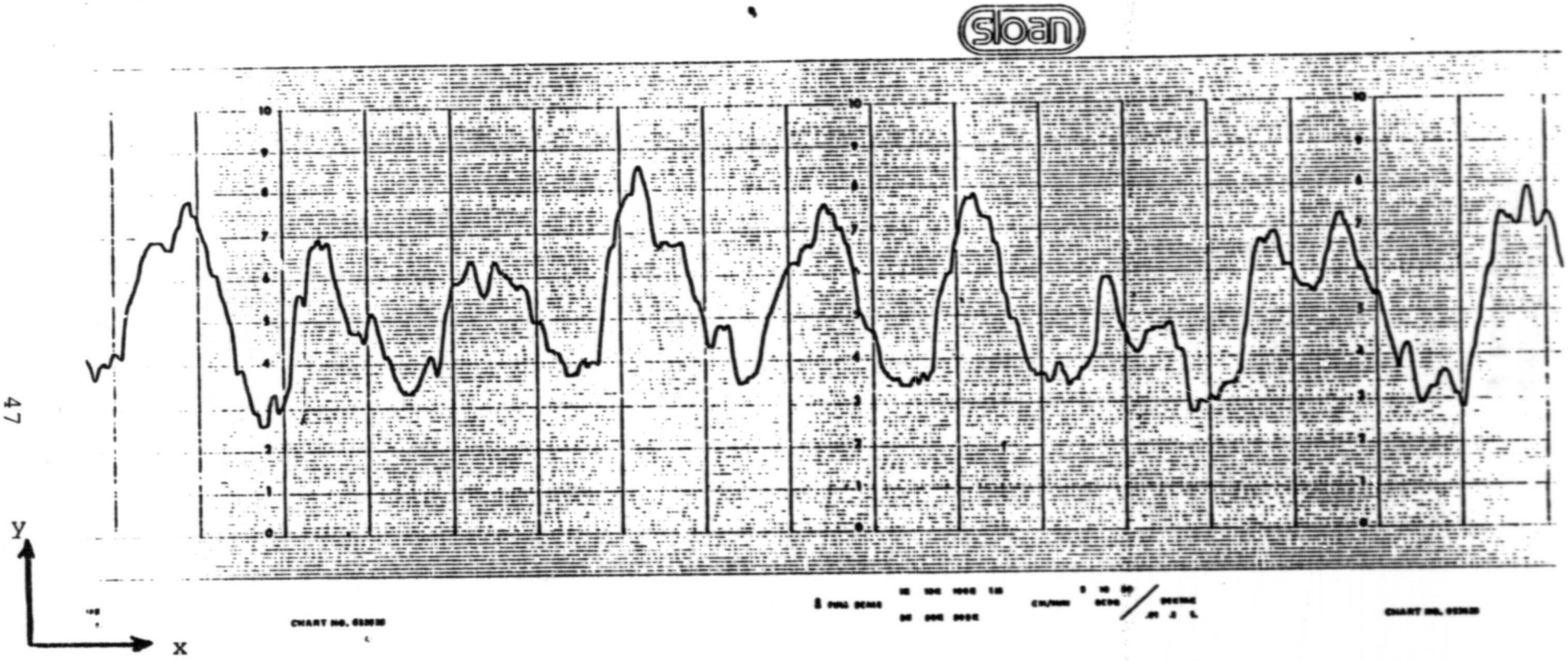

FIG.16B. TYPICAL SURFACE TRACE OF THE ERODED SURFACE AT HIGHER MAGNIFICATION, x = 100 TIMES, y = 1000 TIMES.

ORIGINAL PAGE IS
OF POOR QUALITY

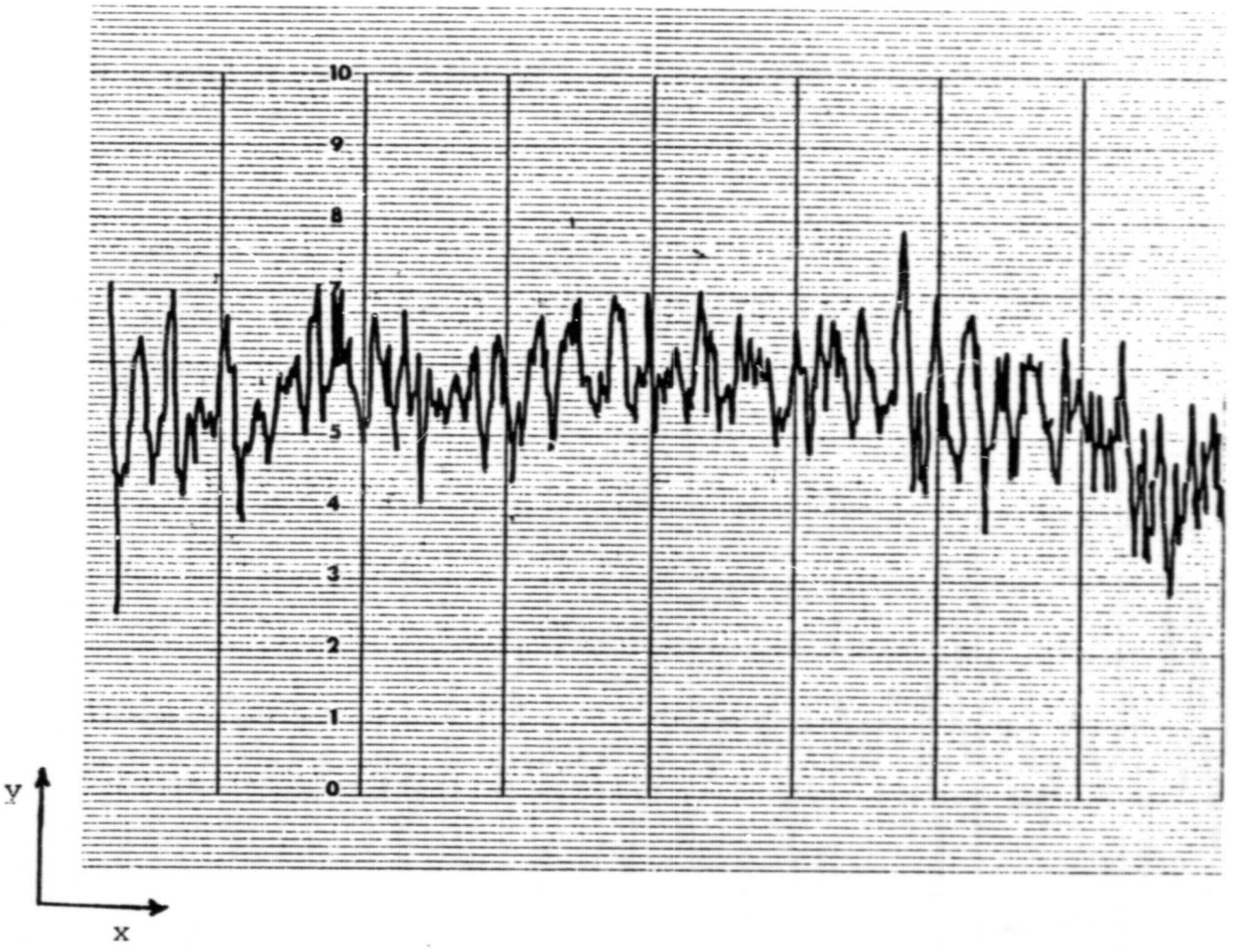

FIG. 17a. SURFACE TRACE OF ERODED SPECIMEN. MAGNIFICATION x = 20 TIMES, y = 1000 TIMES. $\alpha = 45°$, $d_p \simeq 165$ microns. $\dot{m}_{ts} = 10$ gm/cm^2, t = 1.14 min.

ORIGINAL PAGE IS
OF POOR QUALITY

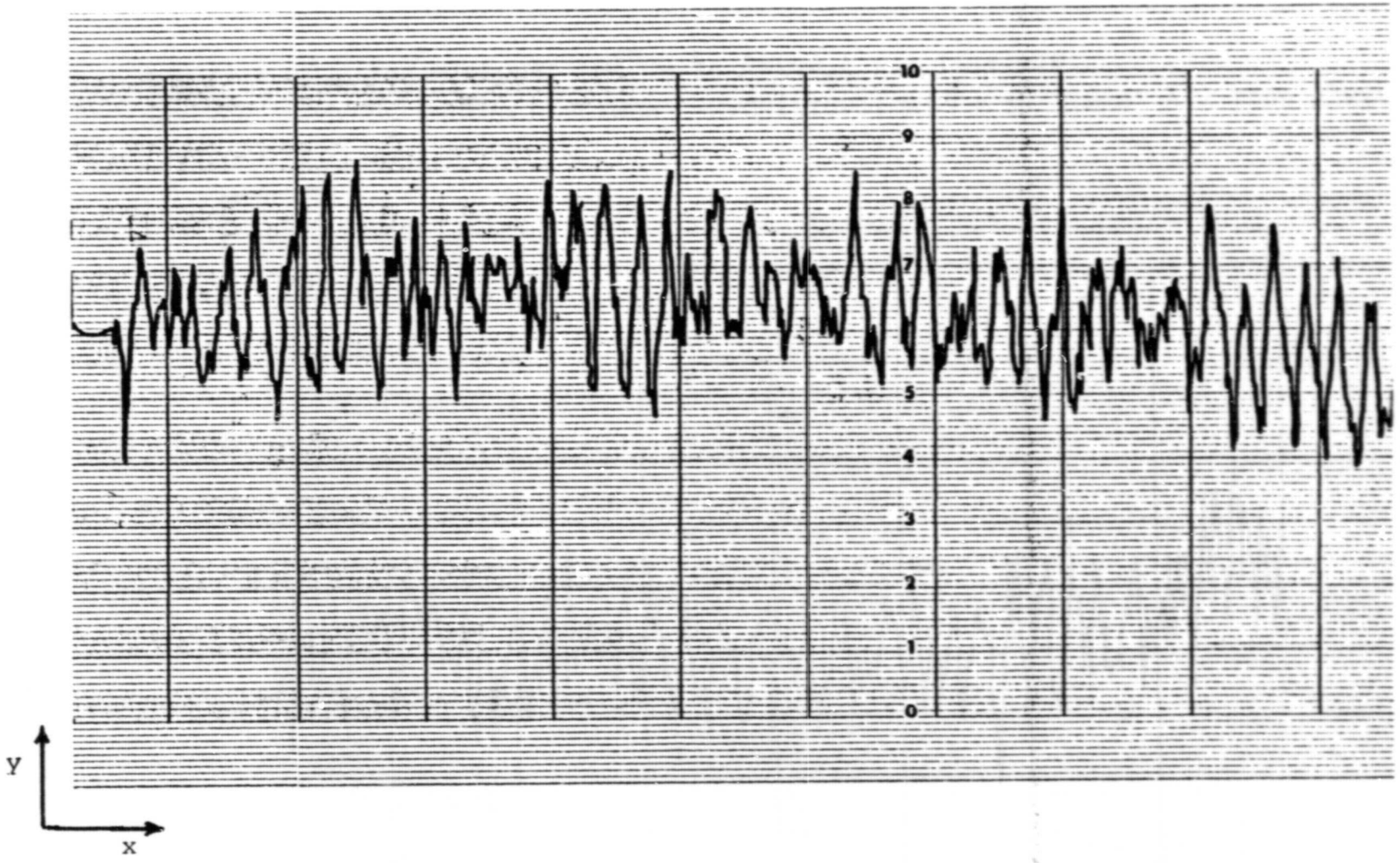

ORIGINAL PAGE IS
OF POOR QUALITY

FIG. 17b. SURFACE TRACE OF ERODED SPECIMEN. MAGNIFICATION x = 20 TIMES, y = 1000 TIMES. $\alpha = 45°$, d_p = 165 microns. $\dot{m}_{ts}$ = 20 gm/cm^2, t = 2.27 min.

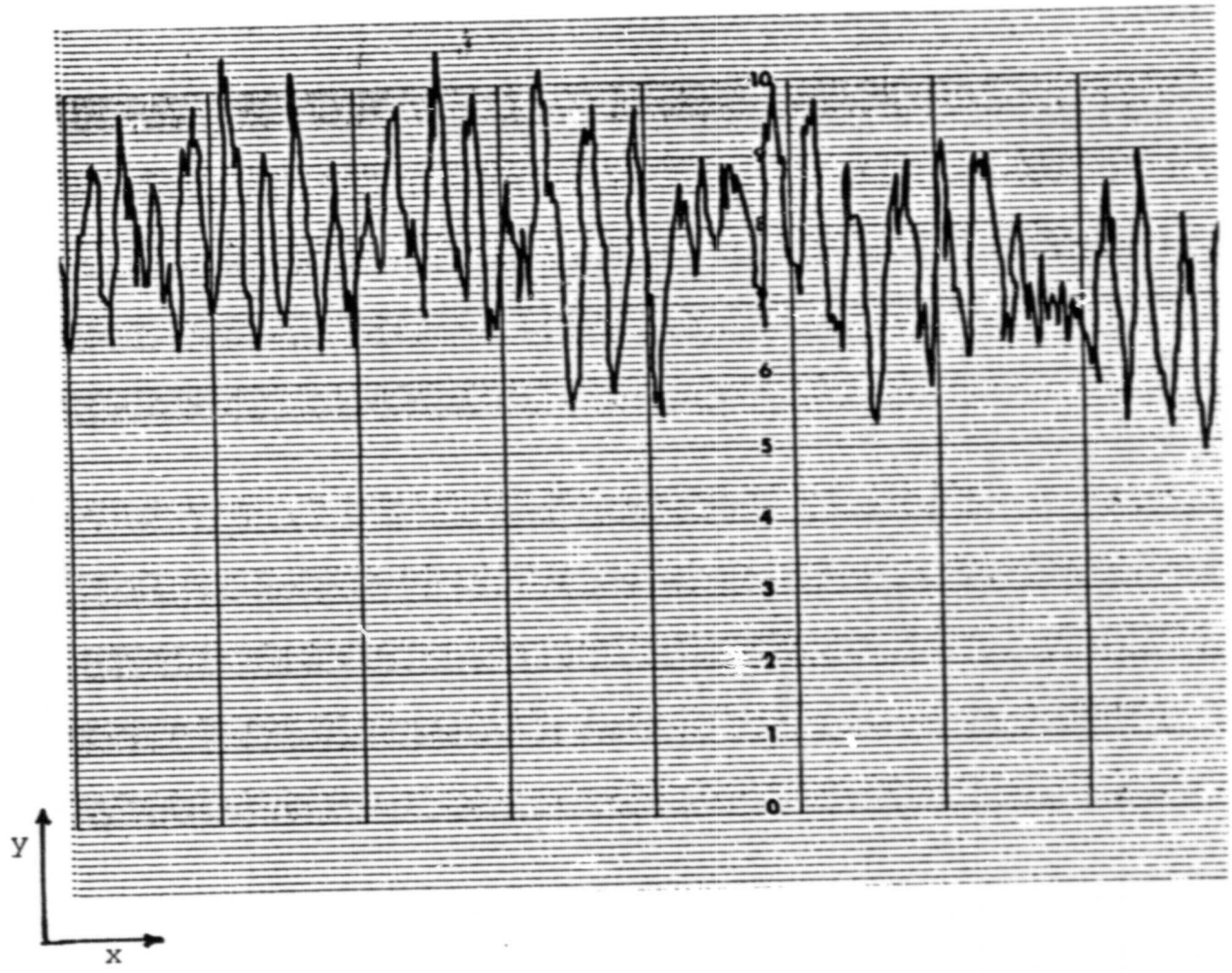

FIG. 17c. SURFACE TRACE OF ERODED SPECIMEN. MAGNIFICATION x = 20 TIMES, y = 1000 TIMES. $\alpha = 45°$, d_p = 165 MICRONS. $\dot{m}_{ts}$ = 40 gm/cm^2, t = 4.55 min.

ORIGINAL PAGE IS
OF POOR QUALITY

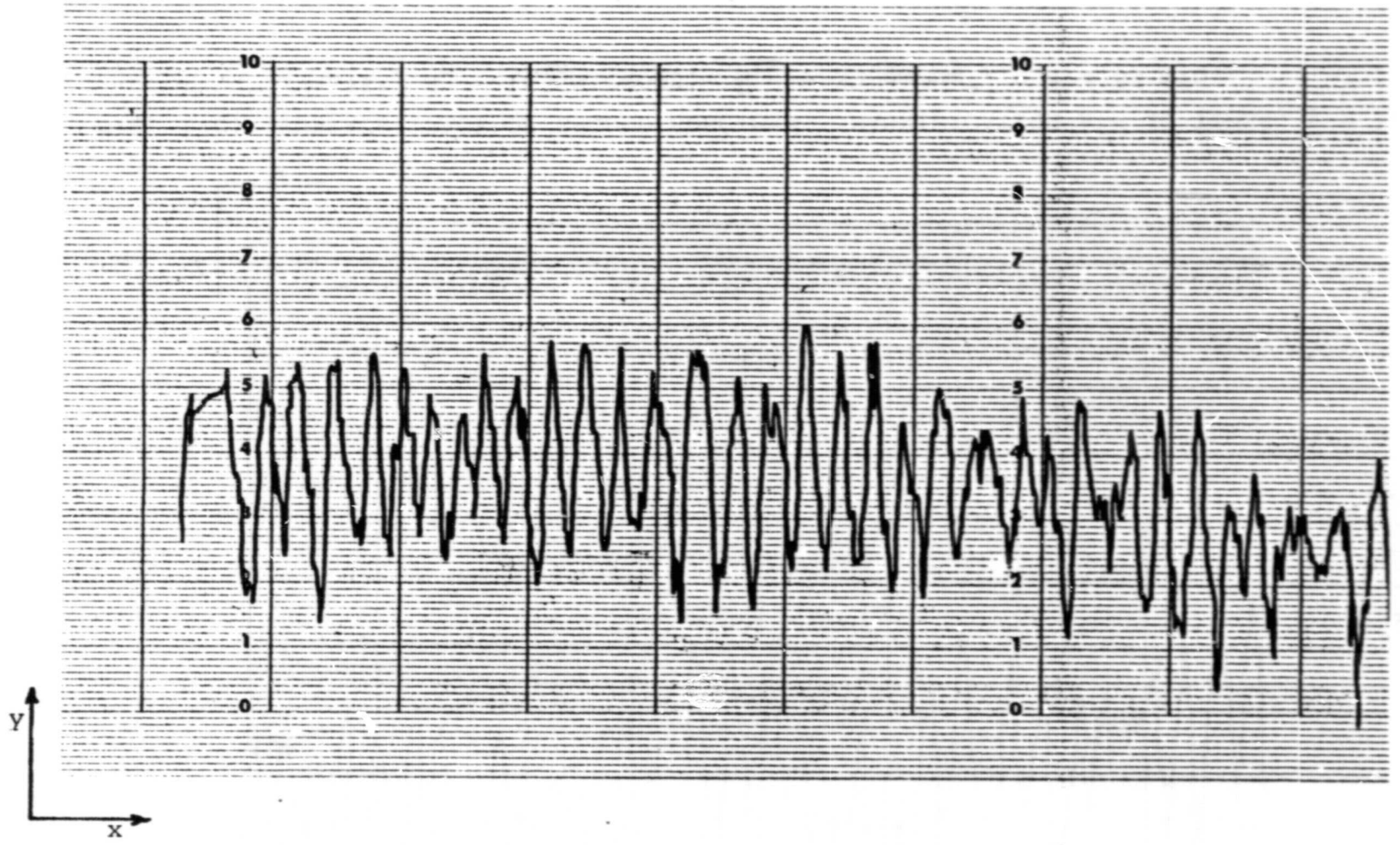

ORIGINAL PAGE IS
OF POOR QUALITY

FIG. 17d. SURFACE TRACE OF ERODED SPECIMEN. MAGNIFICATION x = 20 TIMES, y = 1000 TIMES. $\alpha = 45°$, $d_p = 165$ MICRONS. $\dot{m}_{ts} = 60$ gm/cm^2, t = 6.82 min.

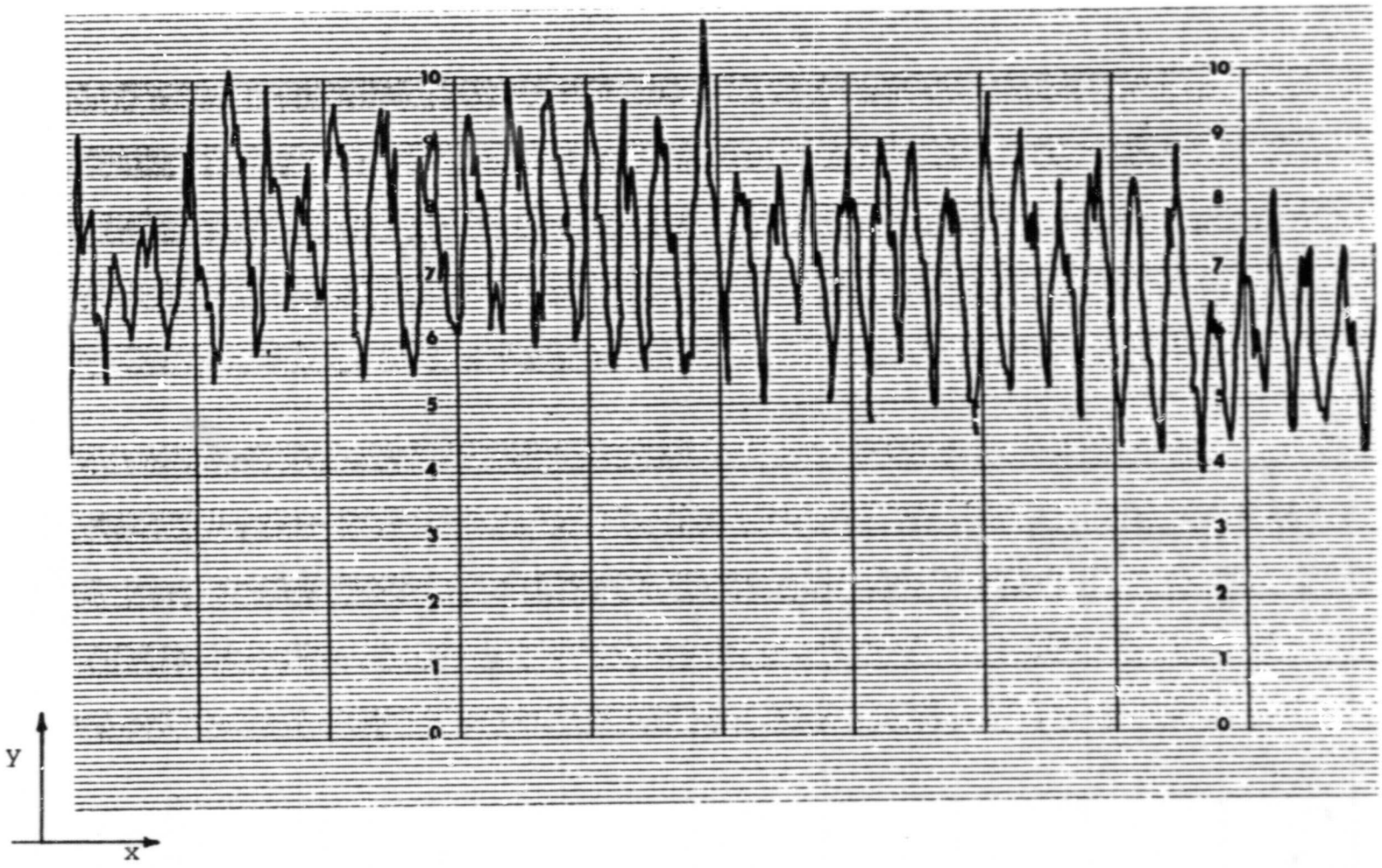

ORIGINAL PAGE IS
OF POOR QUALITY

FIG. 17e. SURFACE TRACE OF ERODED SPECIMEN. MAGNIFICATION x = 20 TIMES, y = 1000 TIMES. $\alpha = 45°$, $d_p = 165$ MICRONS. $\dot{m}_{ts} = 80$ gm/cm^2, t = 9.1 min.

ORIGINAL PAGE IS
OF POOR QUALITY

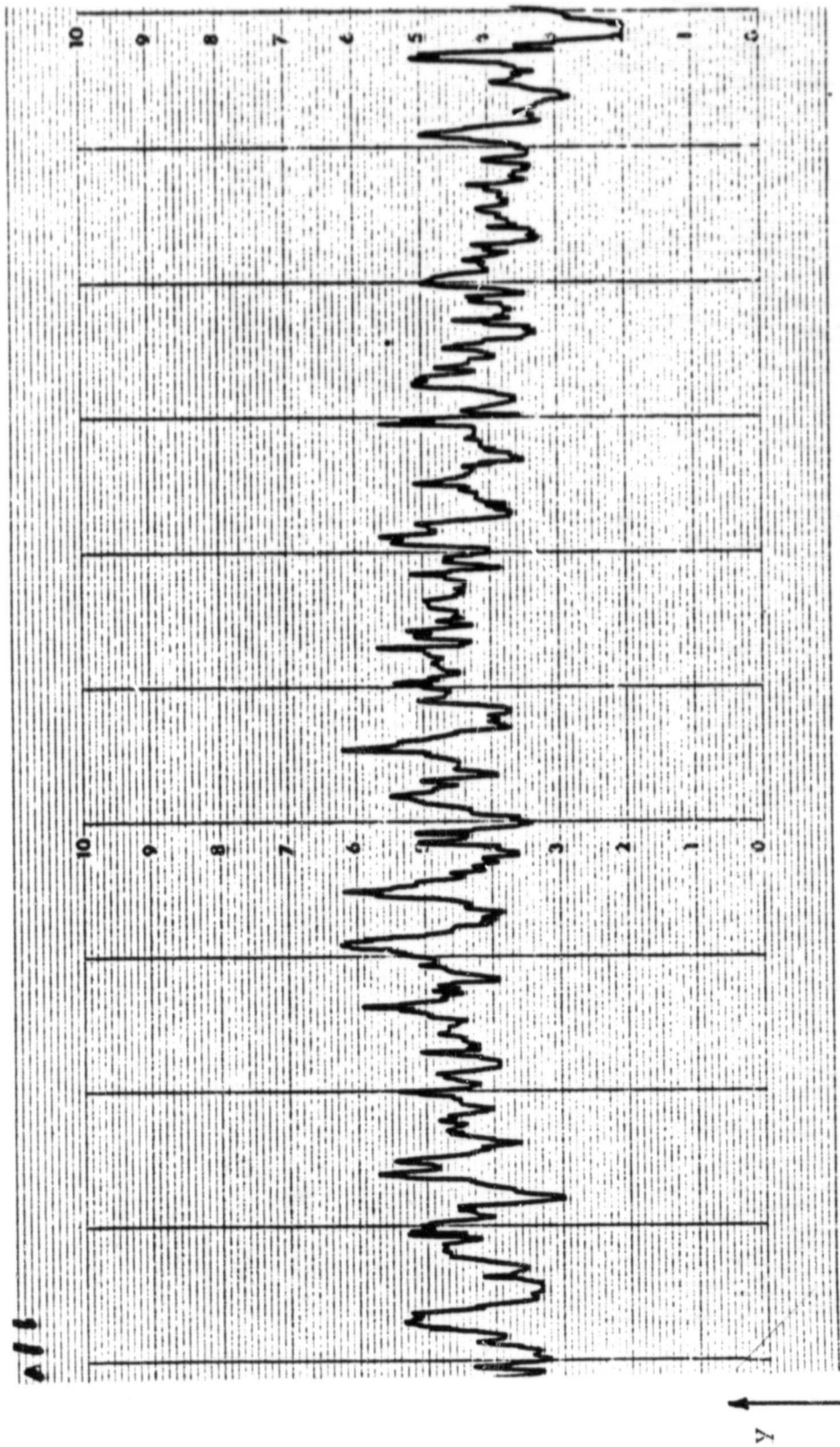

FIG. 18a. SURFACE TRACE OF ERODED SPECIMEN. MAGNIFICATION x = 20 TIMES, y = 1000 TIMES. $\dot{m}_{ts}$ = 124 gm/cm^2, d_p = 225 microns. α = 10°, t = 57.59 min.

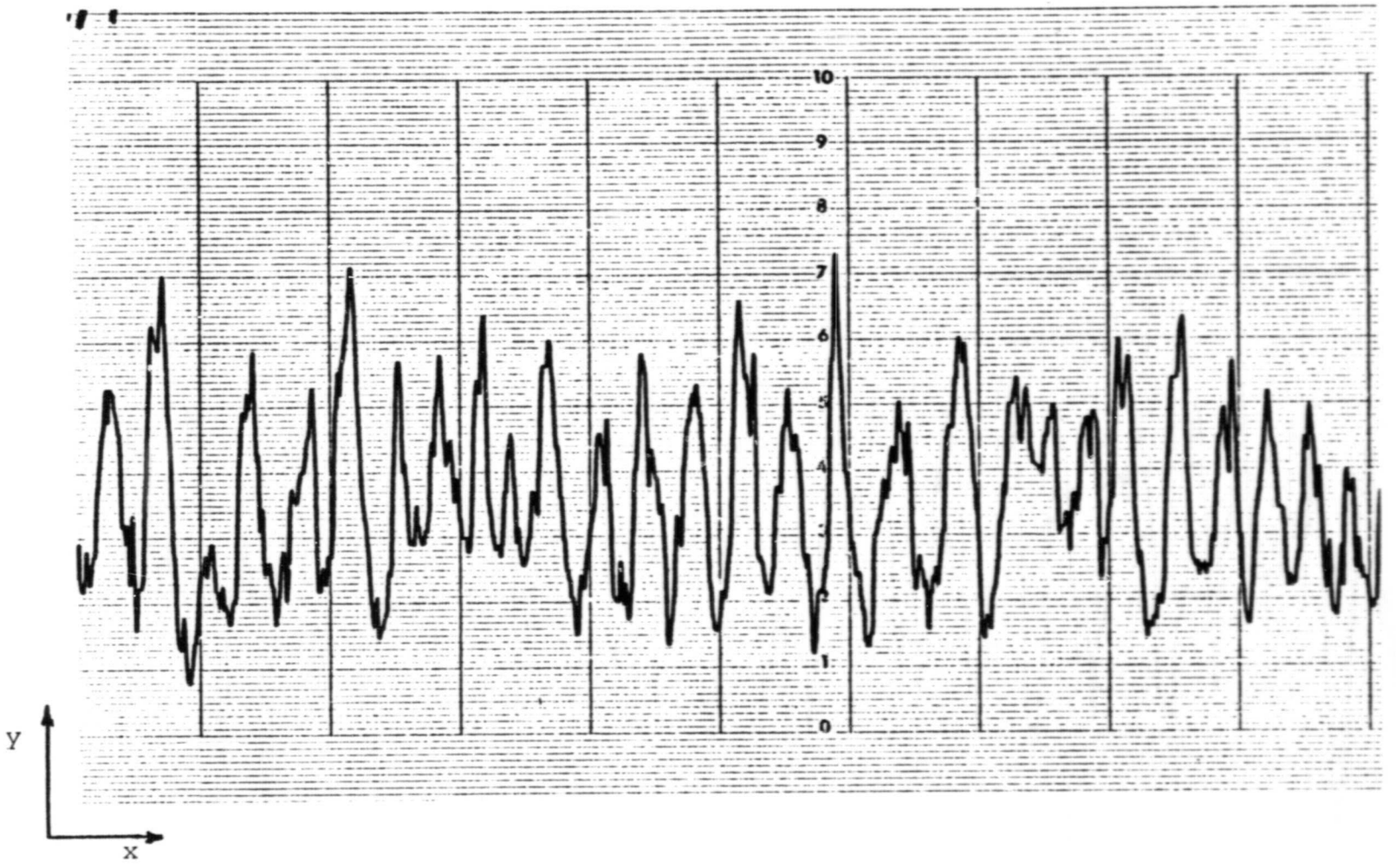

ORIGINAL PAGE IS
OF POOR QUALITY

FIG. 18b. SURFACE TRACE OF ERODED SPECIMEN. MAGNIFICATION x = 20 TIMES, y = 1000 TIMES. $\dot{m}_{ts}$ = 124 gm/cm^2, d_p = 2.25 microns. α = 20°, t = 29.24 min.

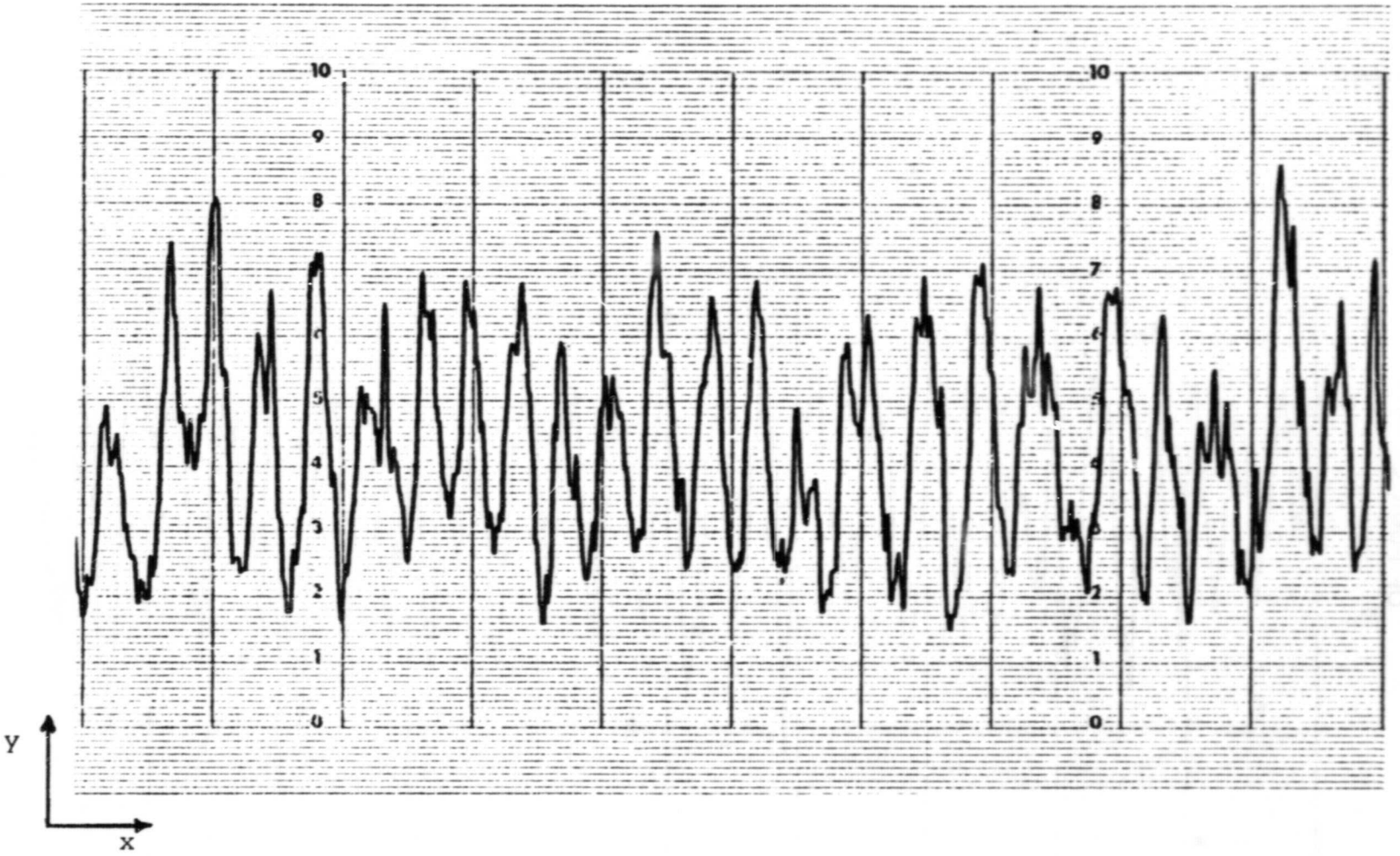

ORIGINAL PAGE IS
OF POOR QUALITY

FIG. 18c. SURFACE TRACE OF ERODED SPECIMEN. MAGNIFICATION x = 20 TIMES, y = 1000 TIMES. $\dot{m}_{ts}$ = 124 gm/cm^2, d_p = 225 microns. α = 25°, t = 23.66 min.

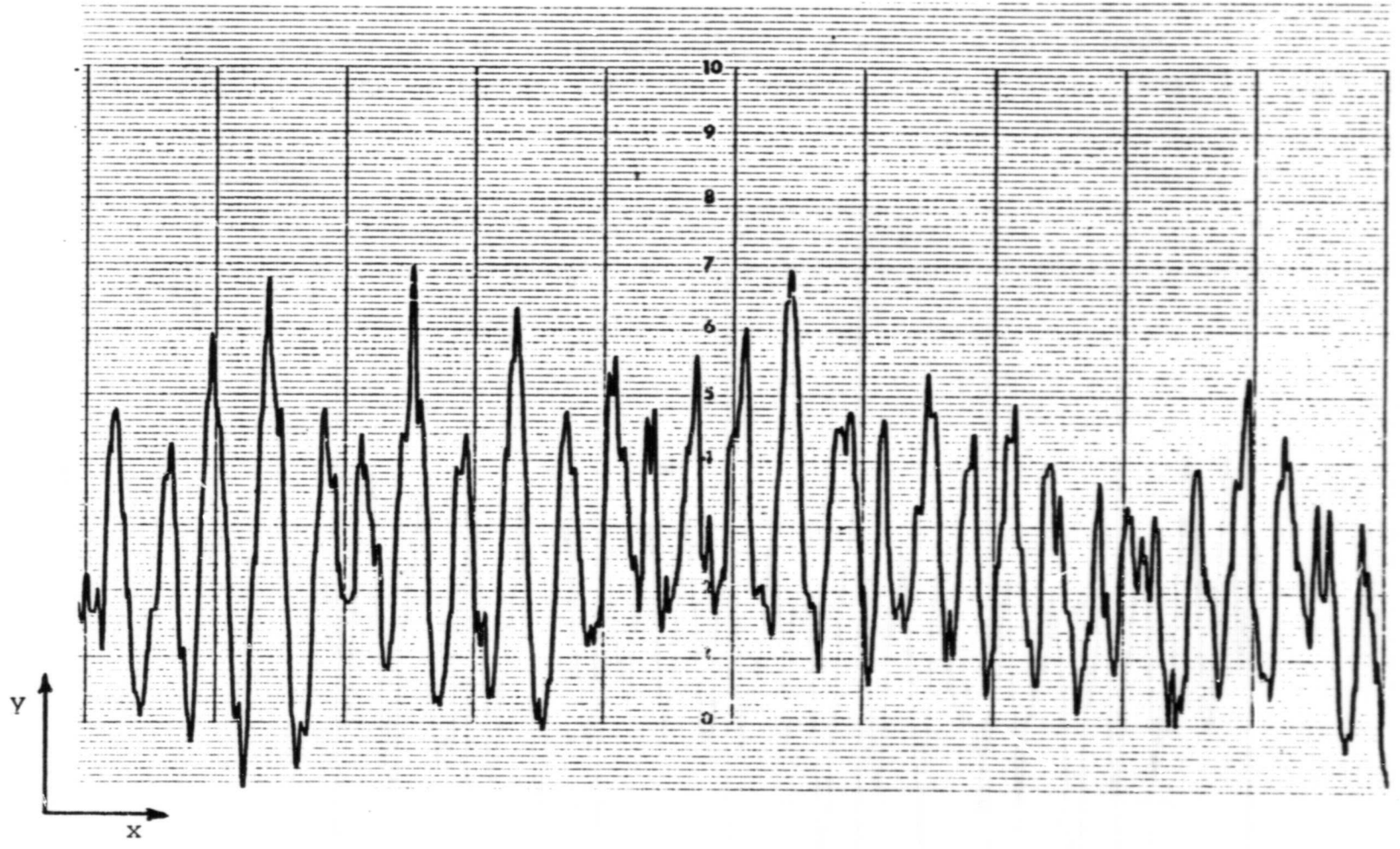

ORIGINAL PAGE IS
OF POOR QUALITY

FIG. 18d. SURFACE TRACE OF ERODED SPECIMEN. MAGNIFICATION x = 20 TIMES, y = 1000 TIMES. $\dot{m}_{ts}$ = 124 gm/cm^2, d_p = 225 microns. α = 30°, t = 20 min.

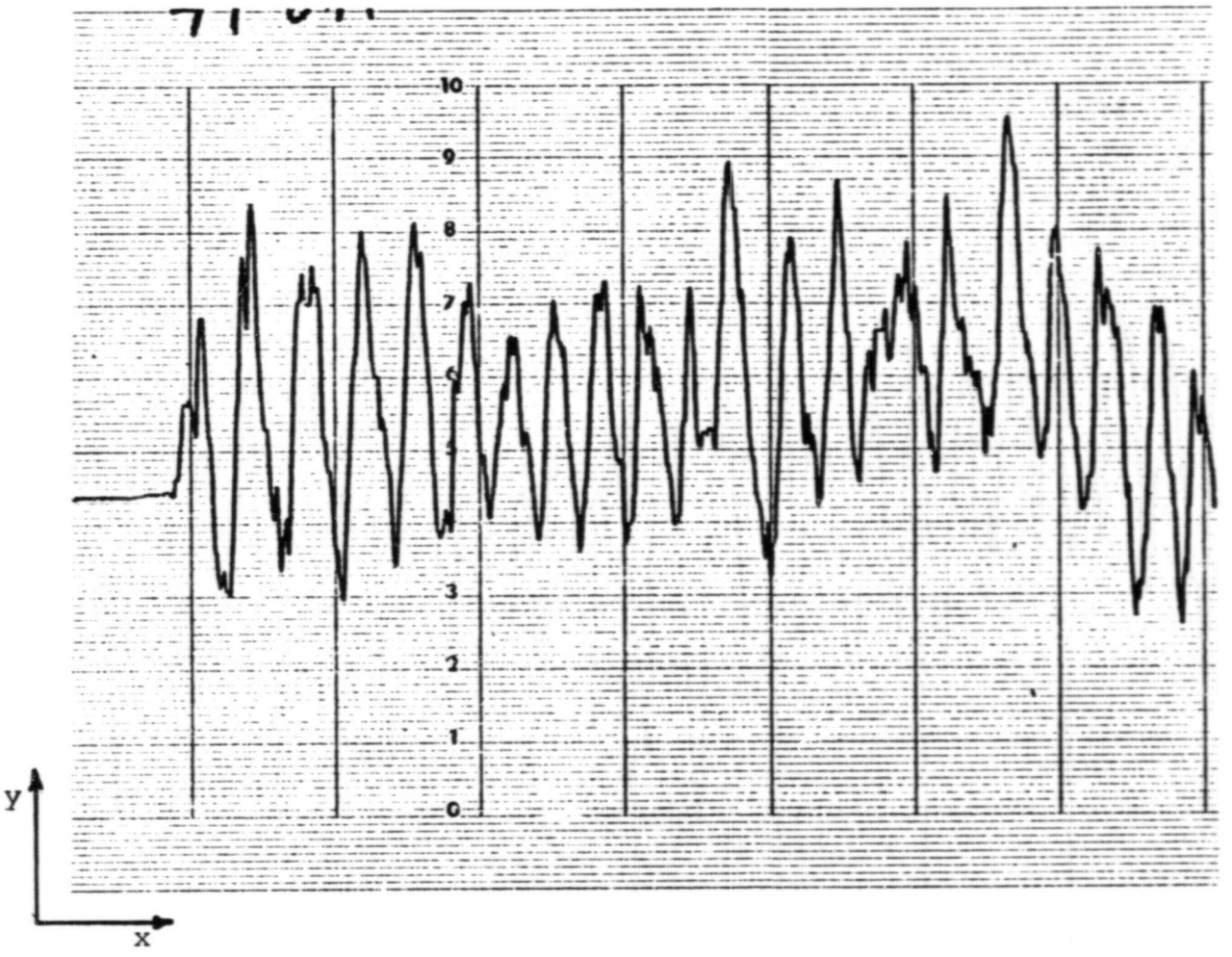

FIG. 18e. SURFACE TRACE OF ERODED SPECIMEN. MAGNIFICATION x = 20 TIMES, y = 1000 TIMES. $\dot{m}_{ts}$ = 124 gm/cm^2, d_p = 225 microns. α = 40°, t = 15.56 min.

ORIGINAL PAGE IS
OF POOR QUALITY

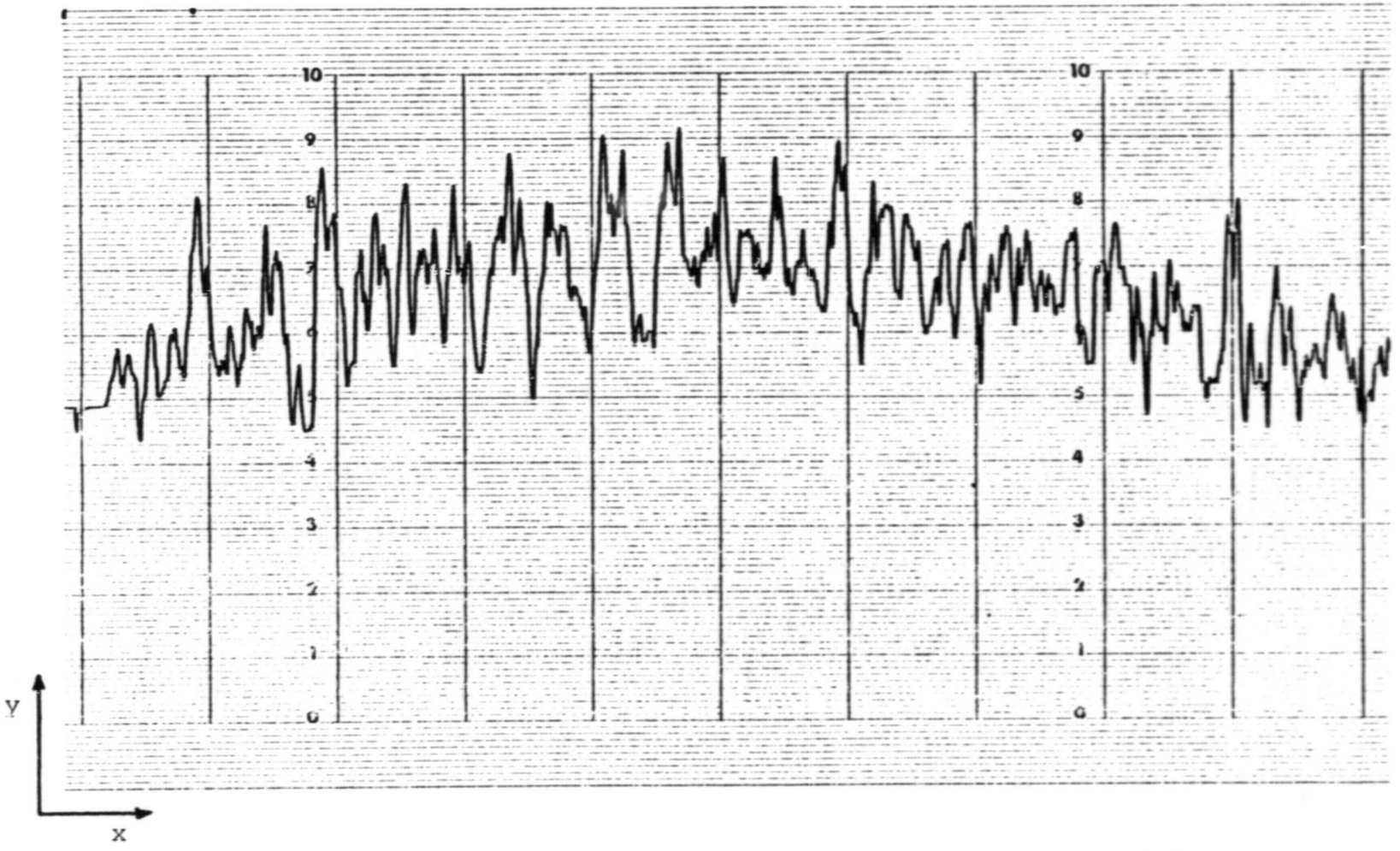

FIG. 18f. SURFACE TRACE OF ERODED SPECIMEN. MAGNIFICATION x = 20 TIMES, y = 1000 TIMES. $\dot{m}_{ts}$ = 124 gm/cm^2, d_p = 225 microns. α = 60°, t = 11.55 min.

ORIGINAL PAGE IS
OF POOR QUALITY

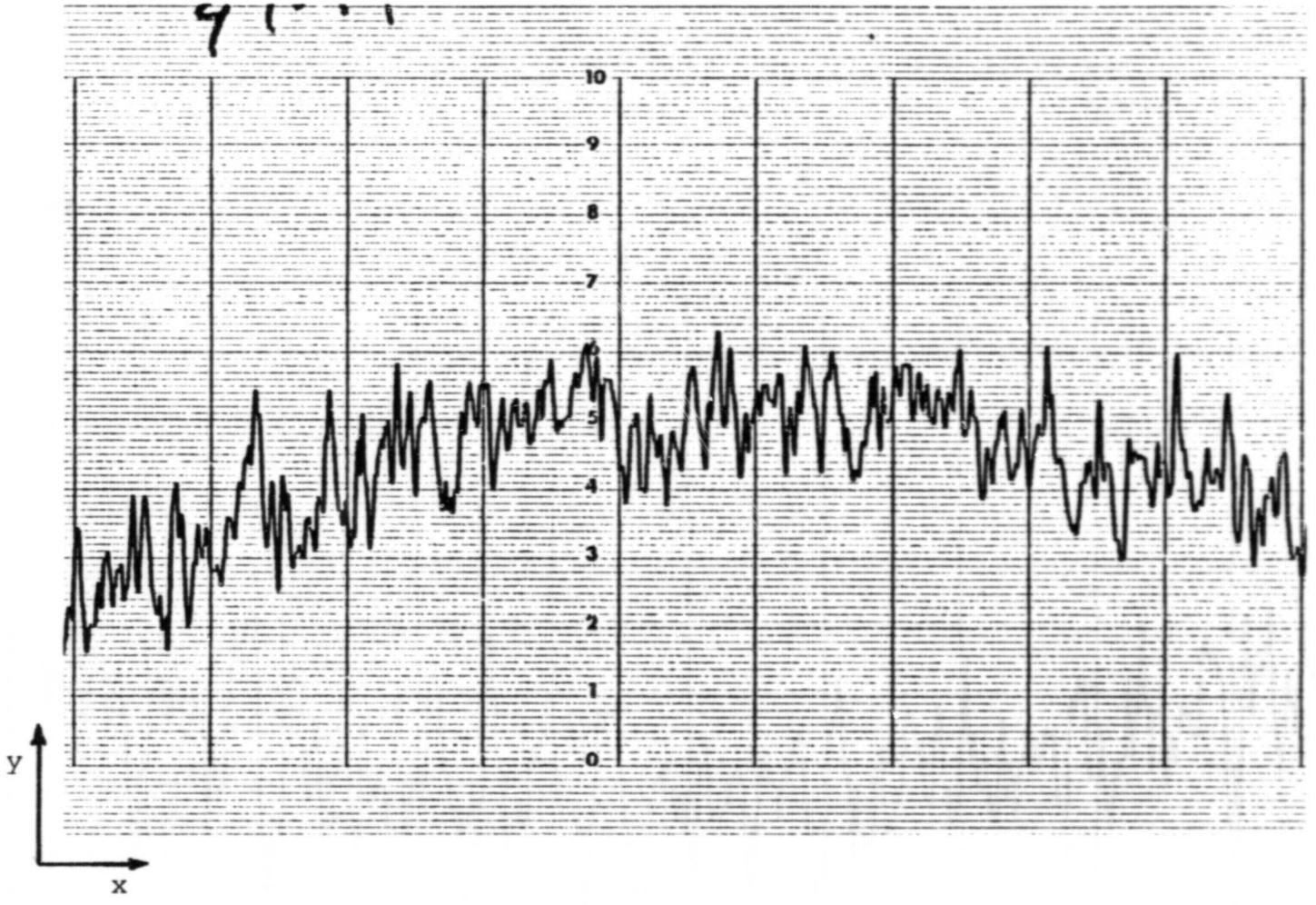

FIG. 18g. SURFACE TRACE OF ERODED SPECIMEN. MAGNIFICATION x = 20 TIMES, y = 1000 TIMES. $\dot{m}_{ts}$ = 124 gm/cm^2, d_p = 225 microns. α = 90°, t = 10 min.

ORIGINAL PAGE IS
OF POOR QUALITY

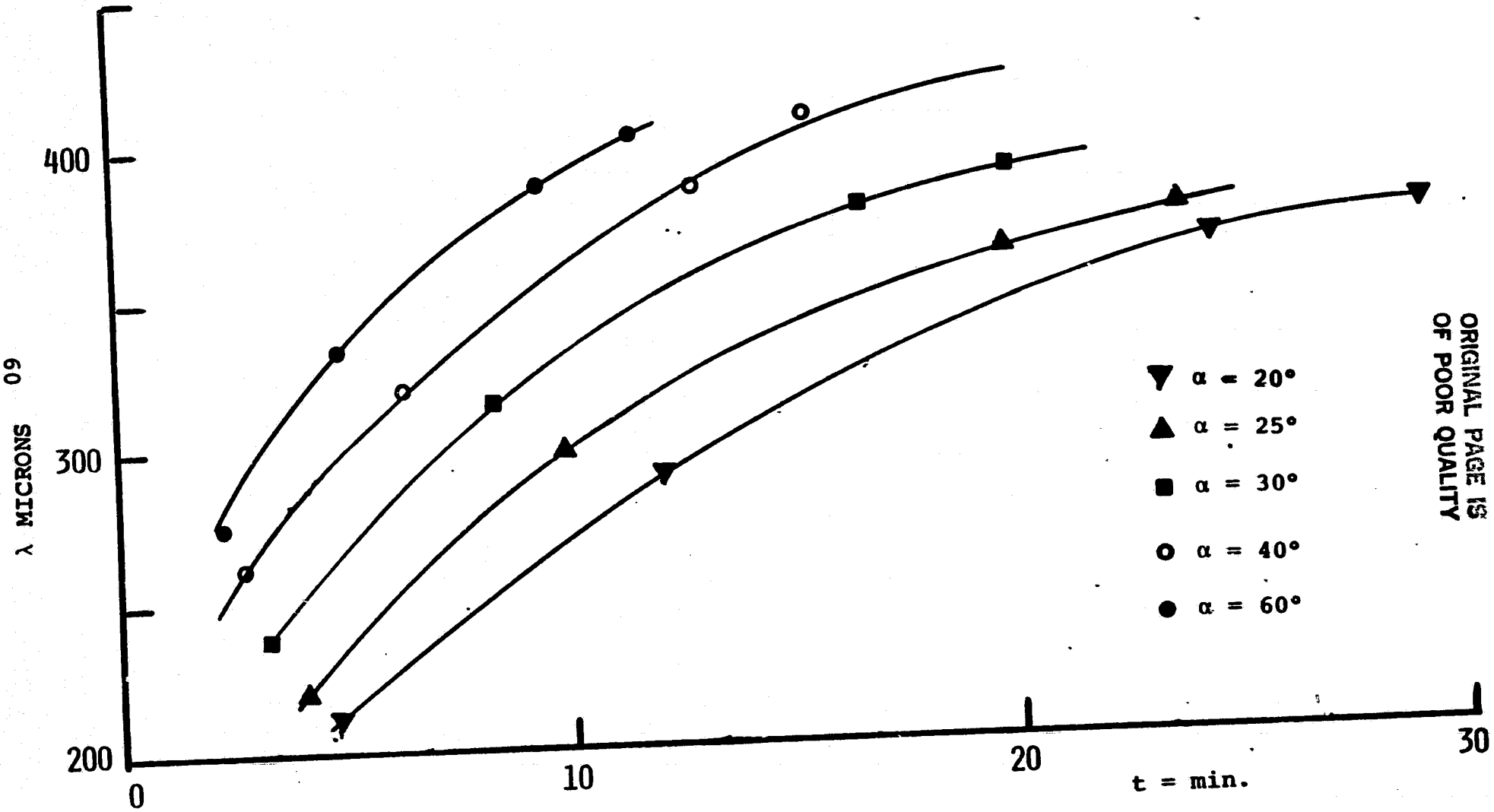

ORIGINAL PAGE IS
OF POOR QUALITY

FIG. 19. MEAN RIPPLE WAVELENGTH VARIATION WITH TIME FOR VARIOUS ANGLES OF ATTACK.
PARTICLE SIZE = 225 MICRONS.

ORIGINAL PAGE IS
OF POOR QUALITY.

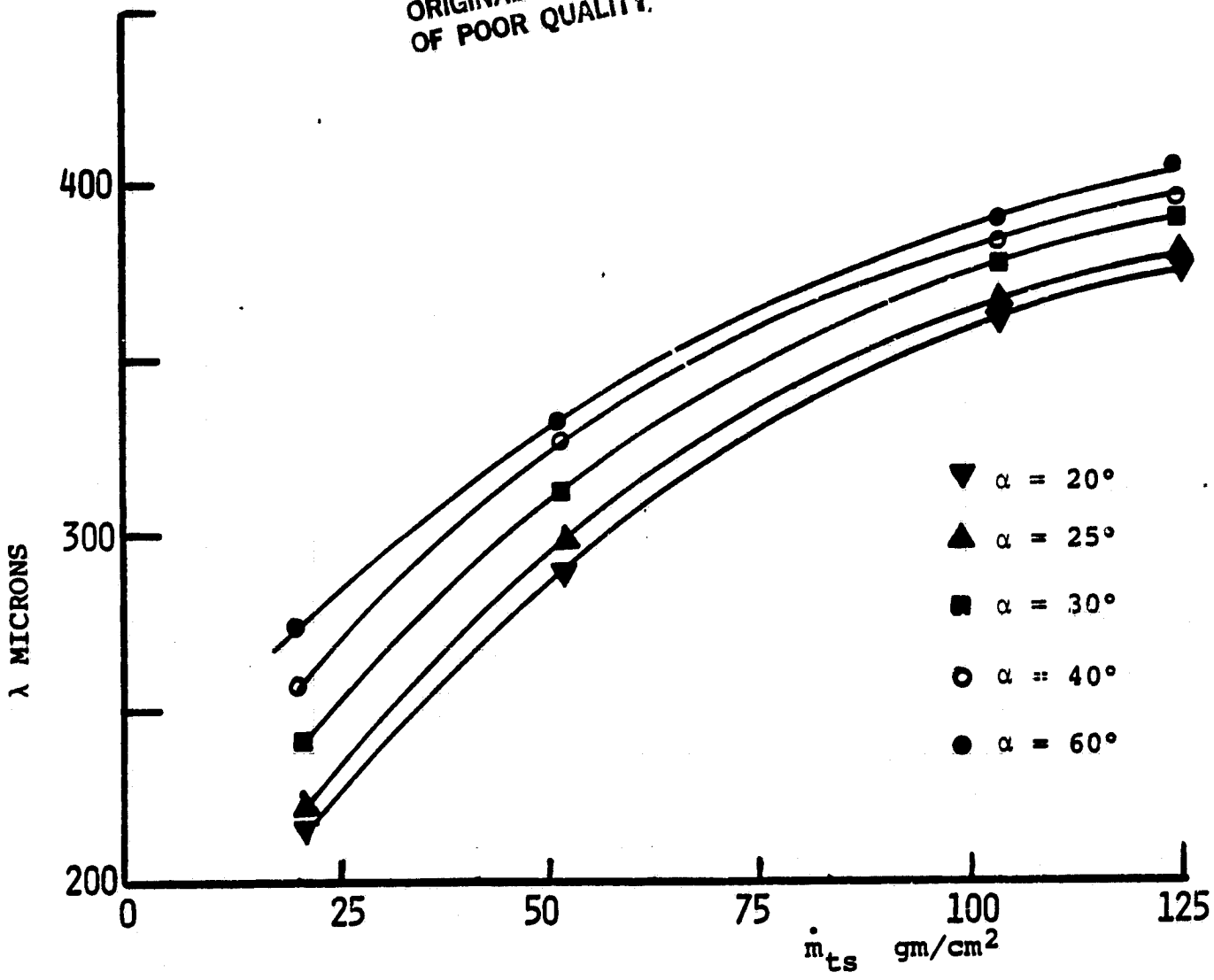

FIG. 20. MEAN RIPPLE WAVELENGTH AS A FUNCTION OF MASS OF PARTICLE IMPACTING. PARTICLE SIZE = 225 MICRONS.

ORIGINAL PAGE IS
OF POOR QUALITY

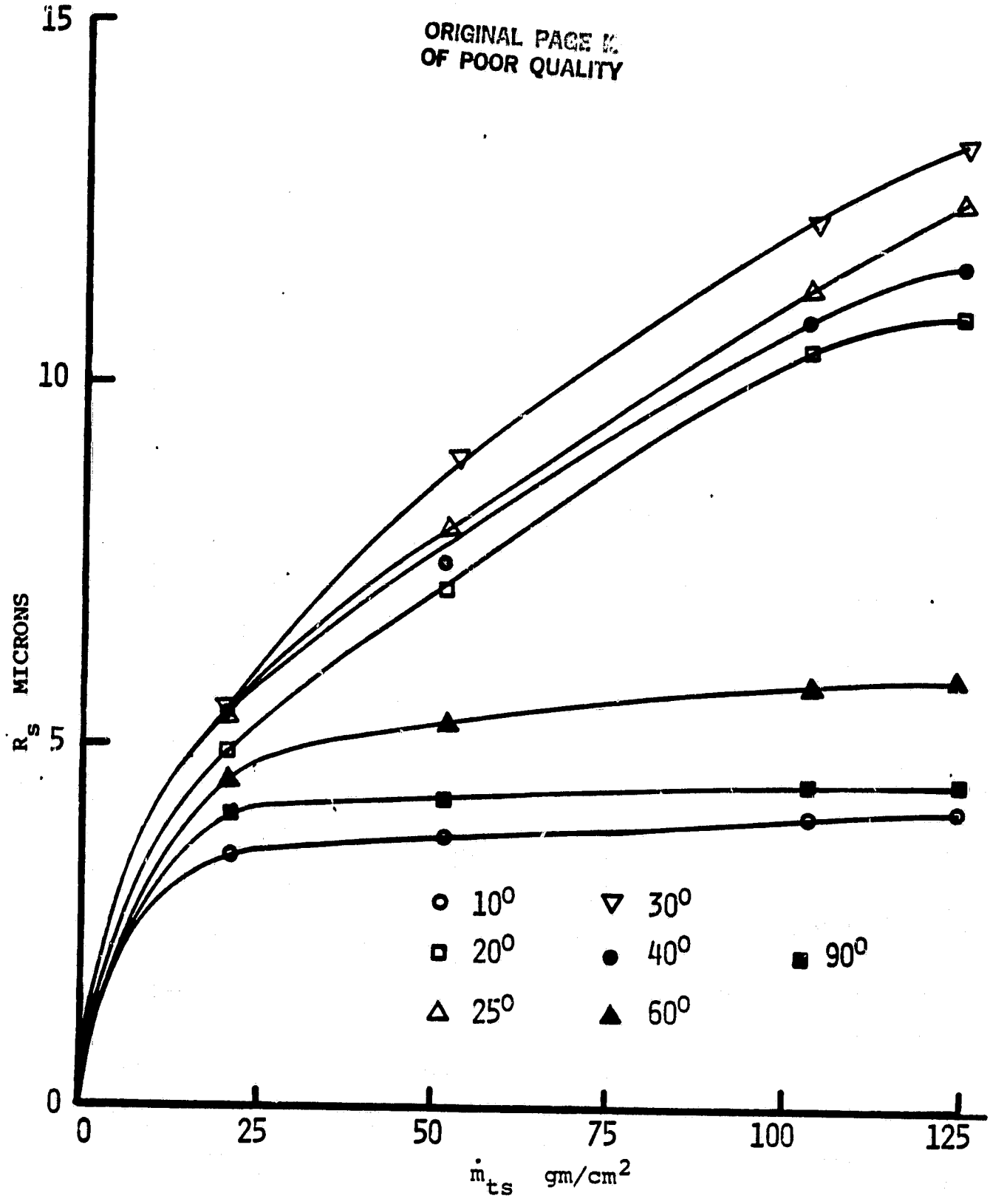

FIG. 21. ROOT MEAN SQUARE, R_s VALUES OF THE ROUGHNESS HEIGHTS AS A FUNCTION OF MASS OF PARTICLE IMPACTING FOR VARIOUS ANGLES OF ATTACK.

ORIGINAL PAGE IS
OF POOR QUALITY

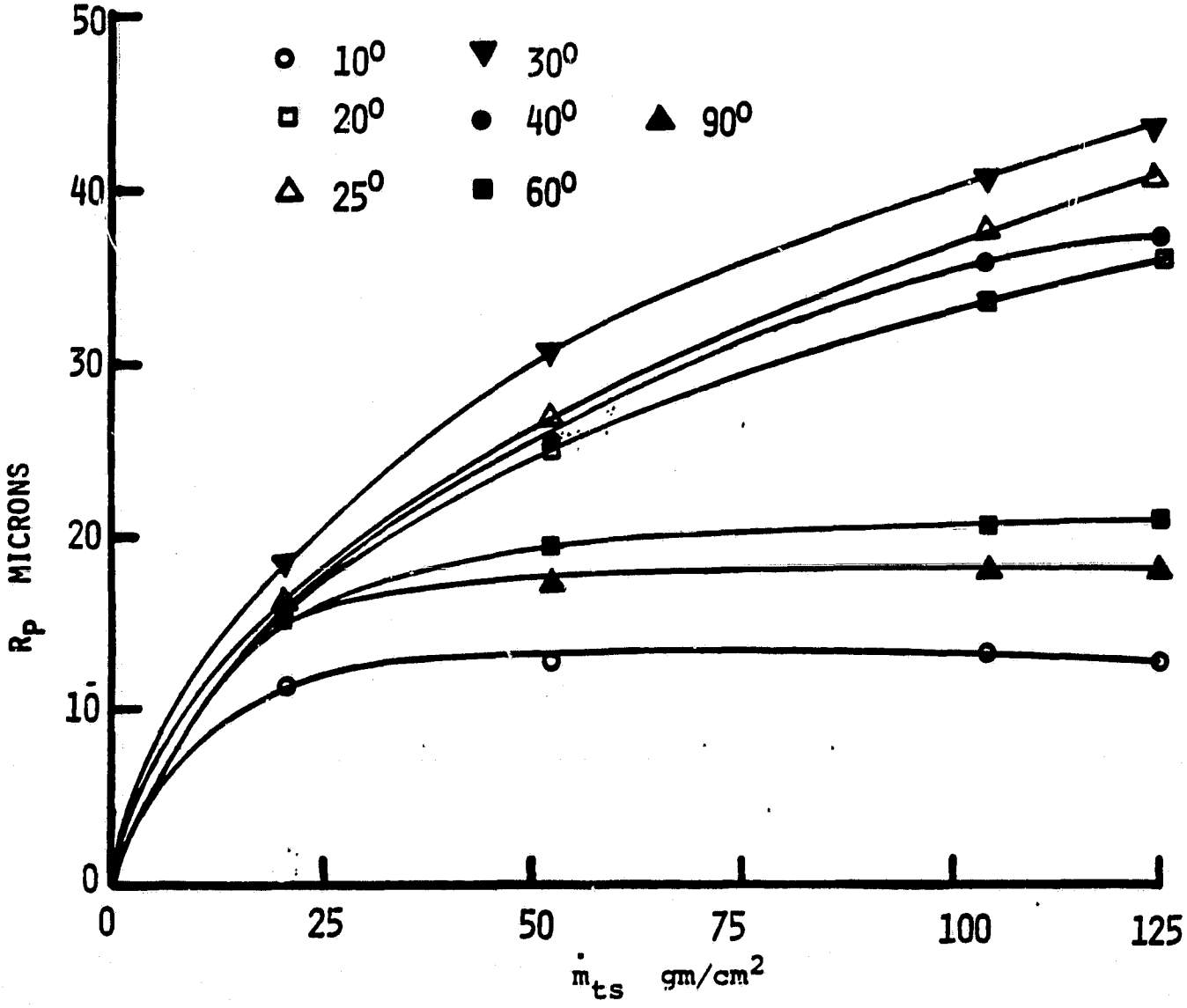

FIG. 22. PEAK TO VALLEY HEIGHTS, R_p OF ROUGHNESS ELEMENTS AS A FUNCTION OF MASS OF PARTICLE IMPACTING FOR VARIOUS ANGLES OF ATTACK.

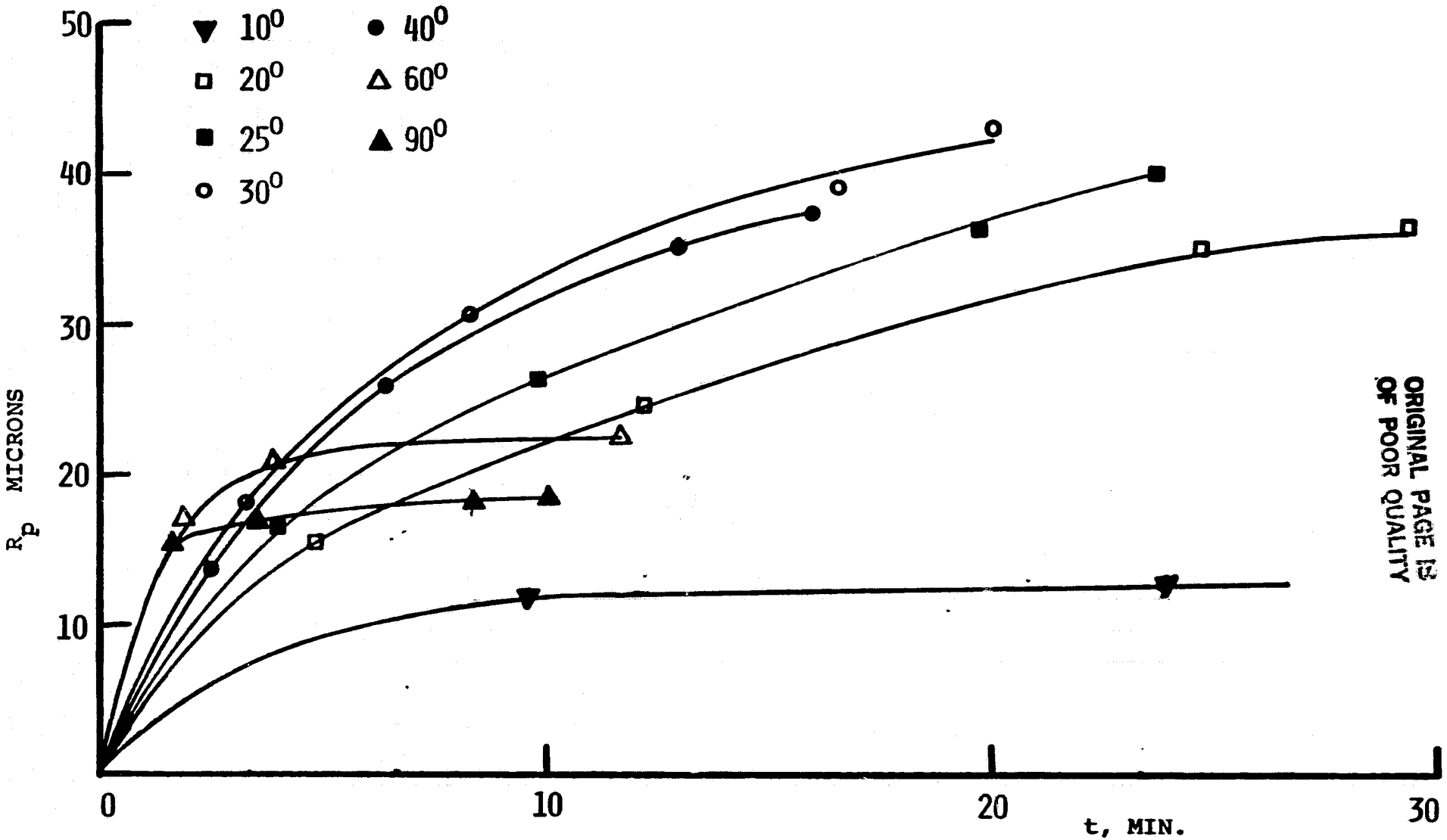

FIG. 23. PEAK TO VALLEY HEIGHTS, R_p OF ROUGHNESS ELEMENTS AS A FUNCTION OF TIME. PARTICLE SIZE = 225 MICRONS.

ORIGINAL PAGE IS
OF POOR QUALITY

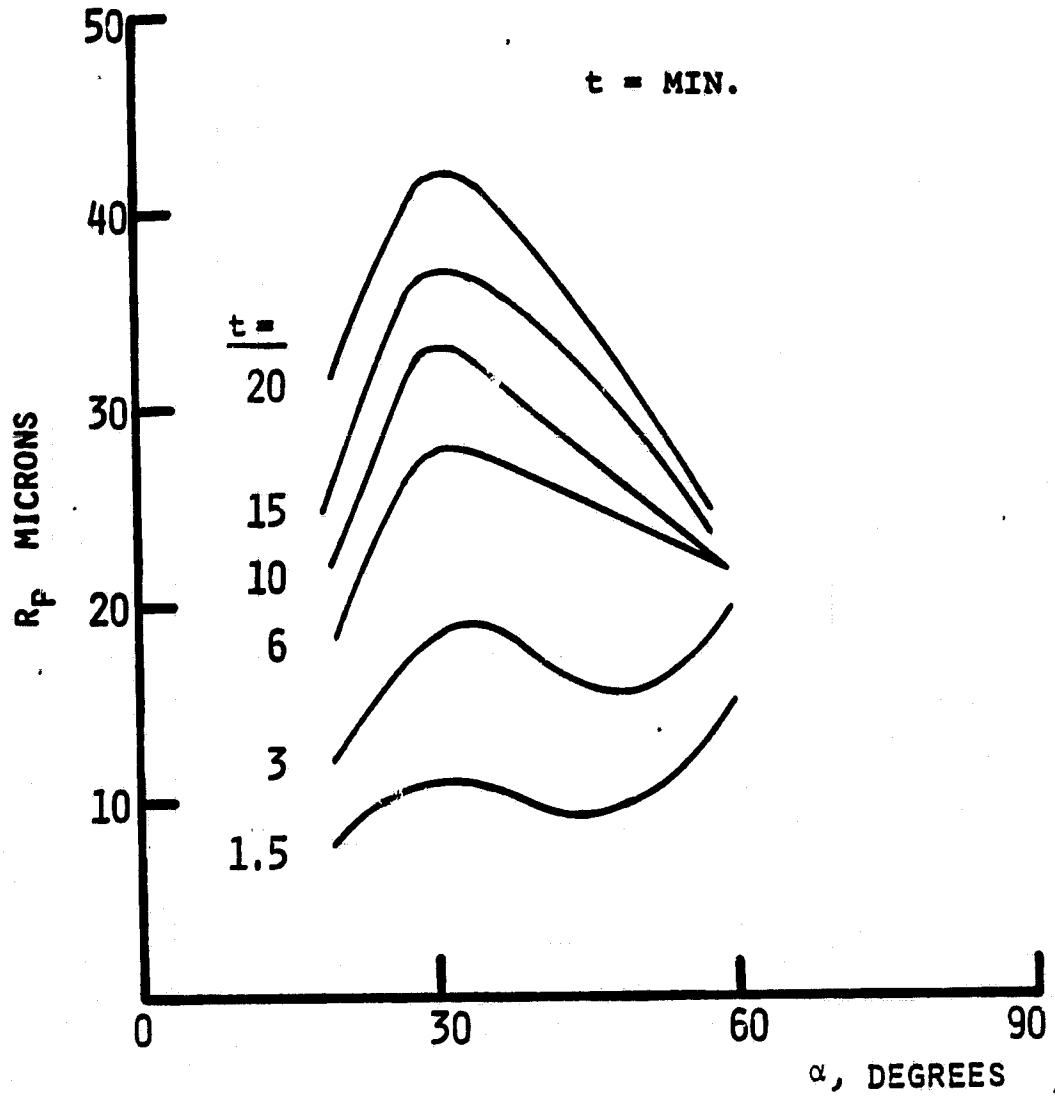

FIG. 24. VARIATION OF ROUGHNESS HEIGHTS, R_p AS A FUNCTION OF ANGLE OF ATTACK FOR VARIOUS TIMES OF EXPOSURE.

ORIGINAL PAGE IS
OF POOR QUALITY

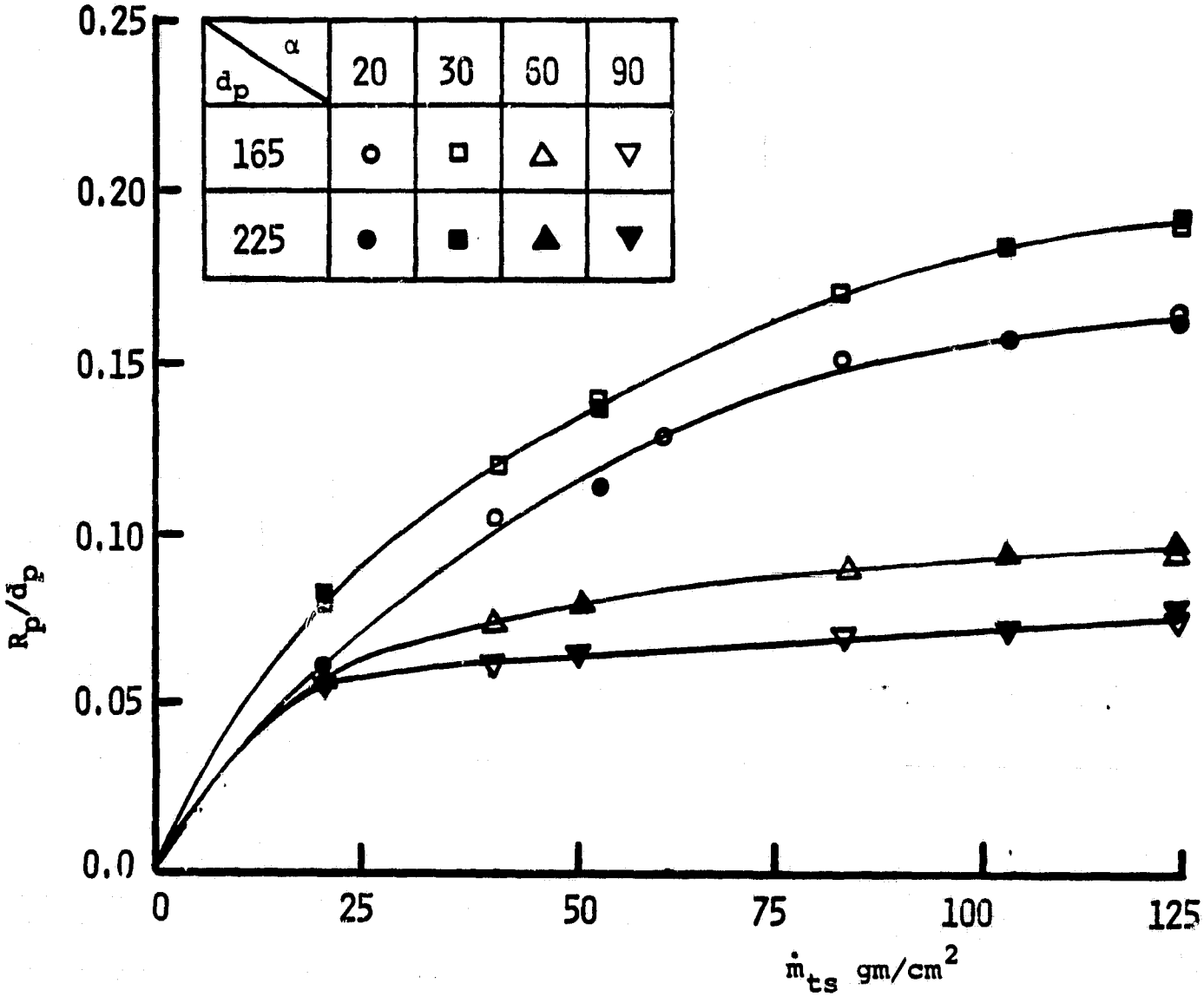

FIG. 25. NONDIMENSIONAL ROUGHNESS HEIGHTS AS A FUNCTION OF THE MASS OF PARTICLE IMPACTING.

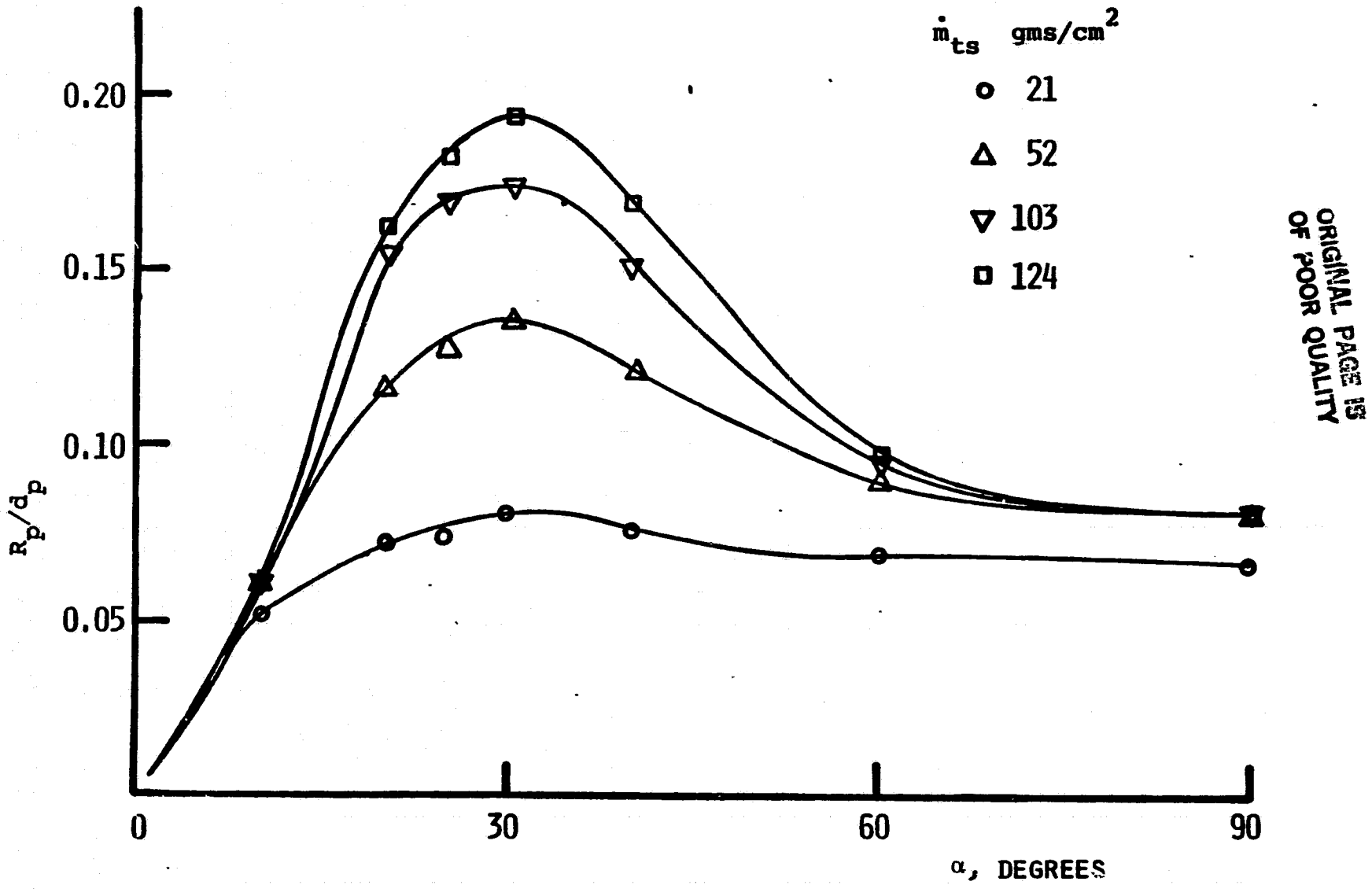

ORIGINAL PAGE IS
OF POOR QUALITY

FIG. 26. VARIATION OF THE NONDIMENSIONAL ROUGHNESS HEIGHTS AGAINST ANGLE OF ATTACK FOR DIFFERENT MASS OF PARTICLE IMPACTING. d_p = 225 MICRONS.